





Cite this: *Energy Adv.*, 2024,  
3, 389

# Graphene-derived composites: a new Frontier in thermoelectric energy conversion

Vaishali Rath, <sup>a</sup> Ranjeet Brajpuriya, <sup>b</sup> Rajeev Gupta,<sup>b</sup> K. P. S. Parmar<sup>b</sup> and  
Ashish Kumar<sup>\*bc</sup>

The demand for eco-friendly power from waste heat using thermoelectric materials has gained significant attention in recent years. Graphene and its functional derivatives are among the most promising materials for thermoelectric energy conversion owing to their remarkable electrical and thermal properties, making them a critical topic of investigation in the field of thermoelectric materials. This review focuses on the current scenario of thermoelectric graphene and its derivatives, including the synthesis, characterization, performance, and assessment of several thermoelectric materials based on graphene, such as graphene, graphene oxide, reduced graphene oxide, and graphene nanoribbons. This review delves into the emerging field of thermoelectric (TE) energy conversion using composite materials derived from graphene. The authors dissect the novelty of this domain by examining recent breakthroughs and consolidating insights into the design, production, and performance of TE materials incorporating graphene. The unique properties of graphene-based materials are emphasized, along with their innovative applications in conjunction with polymers, inorganics, and hybrid structures. In contrast to previous studies, the authors highlight new research endeavors challenging conventional TE materials and demonstrating unprecedented enhancements in electrical conductivity, thermal conductivity, and mechanical robustness offered by graphene composites. This article also underscores recent progress in fabricating graphene-organic and graphene-inorganic composites, demonstrating their potential as thermoelectric materials.

Received 28th October 2023,  
Accepted 6th January 2024

DOI: 10.1039/d3ya00526g

rsc.li/energy-advances

## 1. Introduction

Concerns about the depletion of conventional fossil fuels and a growing awareness of the importance of environment-friendly preservation have become hot topics in green technology in recent years. With the increasing demand for electricity, global warming, environmental pollution, and the greenhouse effect are the issues we are presently facing, and researchers are focusing on energy harvesting-based power generators to reduce these effects. Thermoelectric (TE) technology is an alternative energy-conversion method that uses TE generators to directly transform waste heat into electricity. In recent decades, there has been notable advancements in the field of thermoelectric materials, particularly in improving their performance at high temperatures ( $> 650\text{ }^{\circ}\text{C}$ ). These advancements have made them suitable for applications in waste heat recovery, specifically in high temperature systems, such

as automotive exhaust and nuclear energy production systems.<sup>1,2</sup> However, a considerable portion of waste heat generated by industrial and residential activities and processes is currently being emitted into the environment owing to the limitations of waste heat recovery (WHR) systems. These systems are either prohibitively expensive or lack necessary technological capabilities to effectively capture medium or low-temperature waste heat. Efforts are being devoted to exploring and developing cost-effective, economically viable, and environmentally sustainable waste heat recovery systems utilising thermoelectric materials (Fig. 1(A)). Additionally, the results concerning waste heat recovery per industry are shown in Fig. 1(B).<sup>3</sup> This environmentally friendly energy-saving technique is regarded as a promising means of easing the strain on energy and the environment. Because of their distinct solid-state architecture, TE generators provide several advantages over traditional power generators in terms of durability and simplicity. By 2024, the TE generator market will have grown significantly and will be worth over \$950 million.

Particularly, organic TE generators provide the extra advantages of being lightweight, compact in size, lack mechanical fluids, and low production costs.<sup>4</sup> Because they can directly convert electricity from heat in a steady system whenever there

<sup>a</sup> Department of Chemistry, Applied Science Cluster, UPES, Bidholi, Dehradun, India

<sup>b</sup> Department of Physics, Applied Science Cluster, UPES, Bidholi, Dehradun, India.  
E-mail: vaishali25011996@gmail.com

<sup>c</sup> Department of Physics and Astronomical Science, Central University of Jammu, Sambha, Jammu, J&K, India



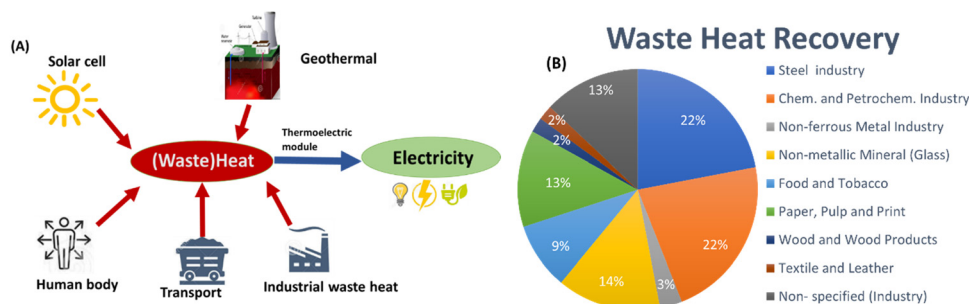


**Fig. 1** (A) Waste Heat Source: since WHR (Waste Heat Recovery) systems are either high-cost or technically unable to recover medium as well as low-temperature waste heat, a sizable portion of the waste heat medium and low temperatures from industrial use, automobiles, residential activities, and processes is still released into the environment. (B) Additionally, the results concerning the waste heat recovery per industry wise. WHR systems based on thermoelectric materials are more economical, less expensive, and environmentally beneficial and are still being sought.

is a temperature difference ( $T$ ) without depending on either light or mechanical action, TEs attract a sizeable share of ongoing research. Additionally, it has a long-life span, requires no maintenance, and may be linked with other energy harvesters. It has been applied for more general purposes, such as satellite manufacturing and planet exploration,<sup>5</sup> owing to the increased heat flux produced by device shrinking, but it has also been used more carefully for various applications, such as the thermal control of micro-nanoelectronic devices.<sup>6</sup> As the use of milli-microwatts of electricity driven by thermoelectrics becomes more common in fields such as micro nanoelectronics,<sup>7</sup> nanoscale robotics,<sup>8</sup> micro electrochemical systems,<sup>9</sup> and wireless telecommunication systems,<sup>10</sup> it is possible to generate electricity from various sources, including industrial, human, and automobile sources.<sup>7</sup> Thomas Johann Seebeck reported the first research study on thermoelectric materials in 1822 based on the Seebeck effect.<sup>11</sup> After that, the Peltier and Thomson effects were described by Peltier<sup>12</sup> and Kelvin<sup>13</sup> in 1834 and 1854, respectively. The development of thermoelectric performance materials slowed in the 20th

century and beyond.<sup>14</sup> Many high-performance TE materials are made of inorganic materials that are expensive, brittle, rigid, heavyweight, and toxic (for example, Bi, Te, and Pb). This inorganic TE material exhibits high-temperature performance. Recent studies have focused on creating inexpensive, cheaper, scalable, adaptable, nontoxic, and lightweight TE materials for use in moderate-temperature applications (300 K to 600 K).<sup>15–17</sup>

Over the past decade, significant developments have been made in organic thermoelectric (OTE) materials with remarkable thermoelectric performance.<sup>18,19</sup> The OTE materials hold promise for various applications because of their unique properties, such as flexibility, cost-effectiveness, environmental friendliness, and tunable characteristics.<sup>20,21</sup> Because of flexibility and lightweightness, OTE materials are often suitable for wearable and flexible electronics and are likely to contribute significantly to the development of energy-efficient technologies and sustainable electronic devices.<sup>22,23</sup> As illustrated in Fig. 2, flexible thermoelectric devices are suitable for portable gadgets and wearables, such as sensors for health monitoring.<sup>4</sup>

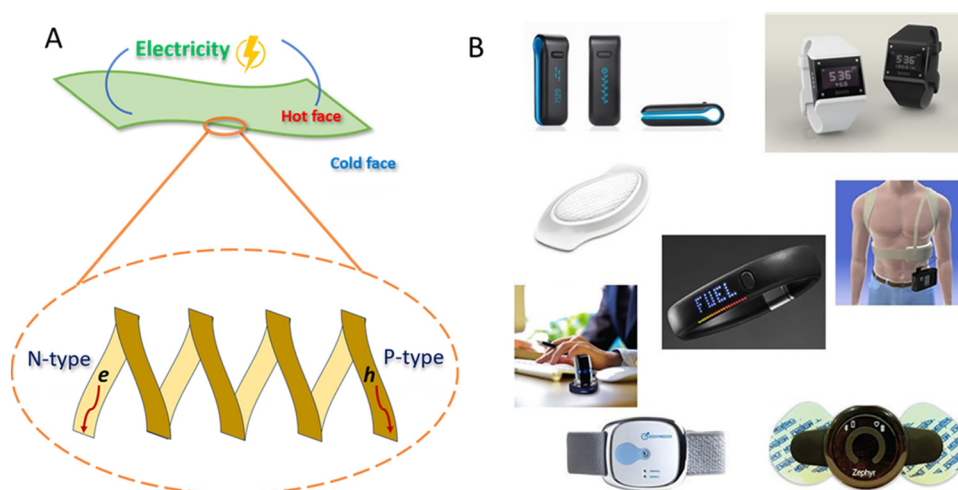


**Fig. 2** (A) A flexible OTE device is depicted, consisting of alternating p-type and n-type semiconducting materials. The device can be made using wearable functional fabric that converts waste body heat into electricity through high energy transfer from a hot face to a cold face. (B) Potential use of organic thermoelectric generators (TEGs) is demonstrated, supporting wearable electronics, such as watches, fitness trackers, health monitoring devices, and toys.



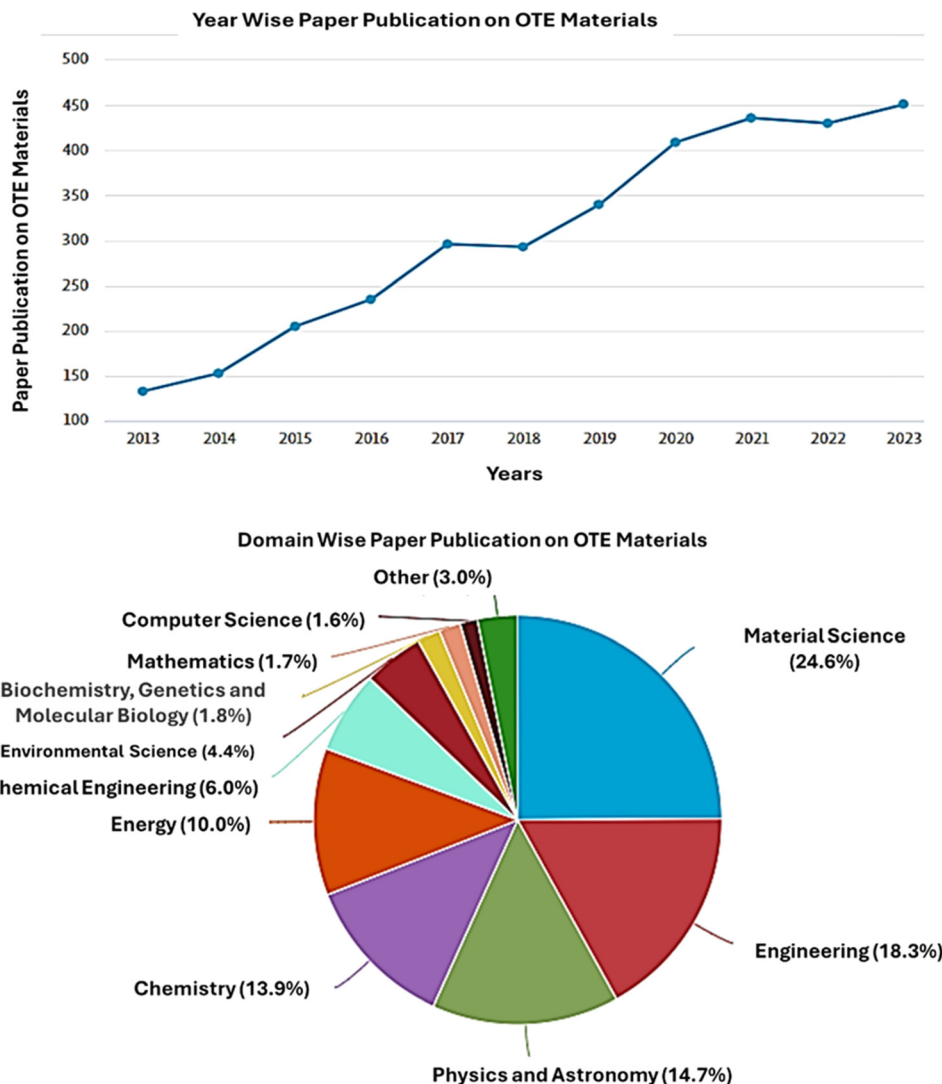


Fig. 3 Year-wise and domain-wise publications on OTE materials.

The cost effectiveness of organic materials is greater than that of their inorganic counterparts.<sup>24,25</sup> They are advantageous because of their large-scale applications in industries where cost is a key consideration.<sup>26</sup> It is possible to chemically engineer organic materials in such a way that they possess specific electronic and thermal properties. Various temperatures and operating conditions can be considered when tailoring the thermoelectric performance of OTE materials.<sup>18,27</sup> Using organic thermoelectric materials, waste heat can be converted into useful electrical power. This could be a future energy harvesting source, along with industrial processes, automobile exhaust, and even human heat.<sup>28,29</sup> It is easy to extract and process organic materials, which allows for a slight environmental impact because they are abundant in environmentally friendly elements.<sup>30</sup> Compared to inorganic materials, organic materials are an environmentally friendly alternative. Materials made from organic compounds are flexible and can conform to complex shapes and surfaces.<sup>31</sup> By adjusting the molecular structure, OTE materials can be tuned owing to their

electronic and thermal properties.<sup>32</sup> A fully organic electronic device can be developed by seamlessly integrating OTE materials with other organic electronic components.<sup>33</sup> By integrating these systems, electronic systems can become more efficient and sustainable.<sup>34,35</sup> For instance, Bubnova, Katz, and other authors provided an excellent overview of the solid-state physics of conjugated polymer compounds.<sup>35</sup> Wang *et al.* recently described several potential OTE materials with maximum power factor (PF) values ranging from  $70 \mu\text{W m}^{-1} \text{K}^{-2}$  to  $2710 \mu\text{W m}^{-1} \text{K}^{-2}$ . In OTE materials, the highest  $ZT$  value achieved is 0.5, as reported in 2015.<sup>36,37</sup> The year-wise and domain-wise publications on OTE show the importance of the materials [Fig. 3].

### 1.1 Thermoelectricity

Thermoelectric generators (TEGs) are used to generate electricity from thermal energy without the need for mechanical components. Thermoelectric devices operate on the principle of the thermoelectric effect, in which the temperature



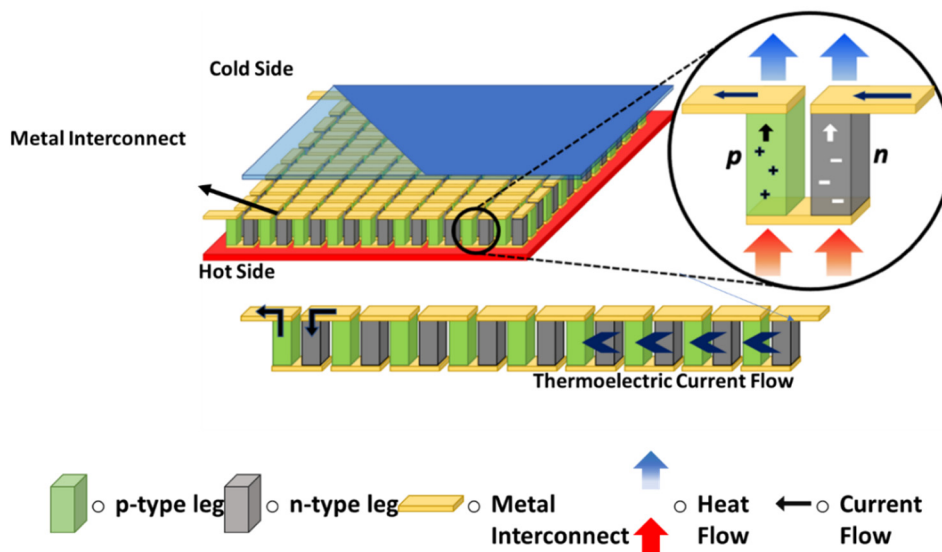


Fig. 4 Diagram depicting the internal structure of various p-type and n-type legs in thermoelectric power generators.

differential is directly converted into electricity. TEGs consist of a few thermoelectric elements typically made of semiconducting materials, which are arranged in a way that creates a temperature difference across them. This temperature difference causes the flow of electrons in the thermoelectric elements, which generates an electrical current. The working principle of TEGs can be explained by considering two legs made of p-type and n-type semiconducting materials. The p-type leg is doped with impurities that create extra holes, while the n-type leg is doped with impurities that create extra electrons. When the TEG is subjected to a temperature difference, the electrons and holes in the two legs are driven to flow in opposite directions, as shown in Fig. 4. This creates a flow of current that can be used to generate electricity.

The efficiency of TEGs depends on the materials used in the thermoelectric elements and the temperature difference between them. Generally, the higher the temperature difference and the better the thermoelectric materials used, the higher the efficiency of the TEG. In a Peltier module, the temperature is lower at the top than at the bottom because heat is removed from the top. The greater temperature at the top of the Seebeck module generates voltage, but the temperature difference has the opposite function in the Peltier module. The materials used in TEGs must also have low thermal conductivity to maintain a temperature difference across thermoelectric elements. Thermoelectric systems can either convert heat into power directly or turn power into a form of cooling.<sup>38</sup>

**TE efficiency.** The TE efficiency of a TE generator is determined by

$$\phi_{\max} = \frac{P_{\text{out}}}{Q_{\text{in}}} \quad (1)$$

where  $P_{\text{out}}$  is the power produced by the device, including heat

losses, and  $Q_{\text{in}}$  is the quantity of heat that enters the device.

$$\phi_{\max} = \phi_c \cdot \frac{\sqrt{1 + ZT_{\text{av}}}}{\sqrt{1 + ZT_{\text{av}}} + T_{\text{h}}/T_{\text{c}}} - 1 = \phi_c \gamma \quad (2)$$

where  $T_{\text{h}}$  is the higher temperature,  $T_{\text{c}}$  is the lower temperature,  $T_{\text{total}} = \left(\frac{T_{\text{h}} + T_{\text{c}}}{2}\right)$ , and the Carnot efficiency is given by  $\phi_c = \left(\frac{T_{\text{h}} - T_{\text{c}}}{T_{\text{h}}}\right) = T_{\text{h}}$ .  $\gamma$  represents the irreversible contribution to efficiency.<sup>39</sup>

The dimensionless figure of merit governs the performance of thermoelectric materials. It is denoted by  $ZT$ :

$$ZT = \frac{S^2 \sigma}{\kappa} \quad (3)$$

where  $S$  represents the Seebeck coefficient,  $k$  represents the thermal conductivity,  $\sigma$  represents the electrical conductivity, and  $T$  represents the absolute temperature. A perfect TE material must have a higher Seebeck coefficient for enhanced energy conversion,<sup>40–42</sup> an increased electrical conductivity  $\sigma$  that decreases the Joule heating effect<sup>43,44</sup> and a poor thermal conductivity ( $\kappa$ ) that can maintain a temperature difference,<sup>45–47</sup> as demonstrated in Fig. 5. It is exceedingly challenging to reach the perfect values for these characteristics, which are connected.<sup>14</sup> For instance, when  $\sigma$  increases,  $S$  typically decreases and  $\kappa$  frequently increases, placing limitations on how much  $ZT$  can be improved. Most of the organic thermoelectric material  $ZT$  used in the 1990s ranged from  $10^{-3}$  to  $10^{-6}$ .<sup>48,49</sup>

Over the past decade, significant developments have been made in organic TEM with remarkable thermoelectric performance. Yu *et al.*<sup>52,53</sup> helped to open the OTE sector for perceptive research on the dissociation between the Seebeck coefficient and electrical conductivity in 2008 and 2010. In





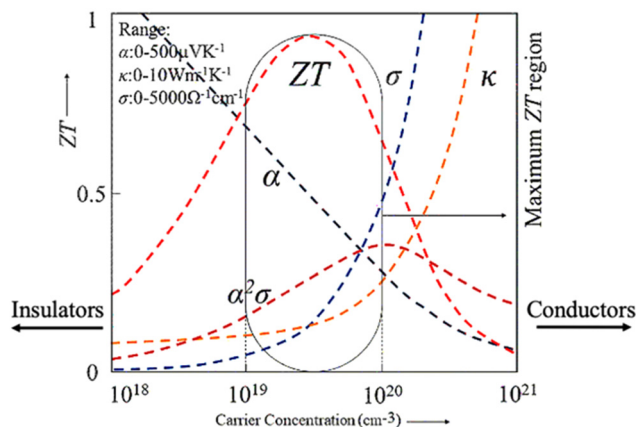


Fig. 5 Thermoelectric parameters with variations in carrier concentration taken from ref. 50, where  $\alpha$  represents the Seebeck coefficient,  $\sigma$  represents the electrical conductivity,  $\kappa$  represents the thermal conductivity, and  $ZT$  represents the figure of merit. The image was adapted with permission from Prasad *et al.*,<sup>51</sup> Springer Nature 2020.

2011, Bubnova *et al.*<sup>54</sup> announced that TE performance had drastically improved, making researchers in related domains quite excited about these findings. Wang *et al.* recently described several potential OTE materials with maximum power factor (PF) values ranging from  $70 \mu\text{W m}^{-1} \text{K}^{-2}$  to  $2710 \mu\text{W m}^{-1} \text{K}^{-2}$ . In OTE materials, the highest  $ZT$  value achieved is 0.5, as reported in 2015.<sup>47,55</sup> Although the maximum  $ZT$  of organic TE at this time is 0.5, it does not compare to inorganic materials, which have a maximum  $ZT$  value of 2.7.<sup>56</sup> A few review papers on OTE materials have been written because of the increasing demand for these materials owing to their potential applications. Organic thermoelectric materials offer various potential applications because of their lower cost and flexibility.<sup>37,49,57–60</sup> For instance, Bubnova, Katz, and other authors provided an excellent overview of the solid-state physics of conjugated polymer compounds.<sup>59,61</sup> Zhang *et al.*<sup>37</sup> summarised the thermoelectric parameters of the most widely used polymers and their composites. Similarly, Toshima *et al.*<sup>60</sup> discussed current developments in organic and hybrid thermoelectric materials that have improved TE performance over the last 20 years. They explain here how to decouple the Seebeck coefficient, and electrical and thermal conductivities to improve the performance of organic thermoelectric materials. Because of the significant link between these factors, the production performance of OTE materials is high. Several strategies have been presented or applied to separate the factors and enhance the functionality of OTE materials. For instance, an altered DOS (density of state) due to quantum confinement increases  $S$  without decreasing  $\sigma$ .<sup>62</sup> Without significantly lowering electrical conductivity, phonon scattering can assist in lowering  $\kappa$ .<sup>63</sup> These three parameters can be regulated further using low-dimensional nanostructures.<sup>64,65</sup>

## 1.2 Organic thermoelectric (OTE) materials

Over the past few years, OTE materials have garnered considerable interest owing to their inherent benefits over traditional

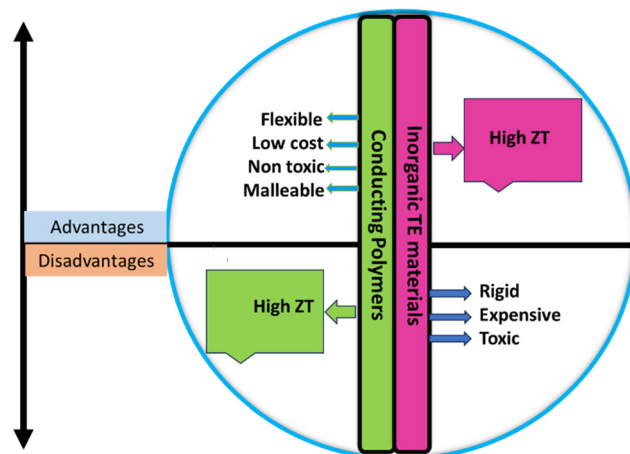


Fig. 6 Schematic representing the comparison between inorganic TE materials and conductive polymers.

inorganic thermoelectric materials. These OTE materials possess various benefits, including low cost, ease of fabrication, lightweightness, minimal toxicity, and low thermal conductivity, as shown in Fig. 6. However, the commercialization of OTE generators has been limited by their poor thermoelectric performance. To improve the efficiency of OTE materials, several key parameters must be considered and optimised.

**1.2.1. Seebeck coefficient and electrical conductivity.** The correlation between the Seebeck coefficient and electrical conductivity is typically attributed to the carrier concentration shown in eqn (4). One commonly employed method for improving the thermoelectric efficiency of the material is to find the highest PF ( $S^2\sigma$ ) by adjusting the concentration of the charge carrier ( $n$ ). A concept commonly employed to explain electron transport in metals can be used to explain the relationship between the Seebeck coefficient and the carrier concentration of strongly conducting materials:<sup>66</sup>

$$S = \frac{8\pi^2 k_B^2}{3eh^2} m^* t \left( \frac{\pi}{3n} \right)^{2/3}, \quad (4)$$

where  $k_B$  is the Boltzmann constant with a value of  $1.3806 \times 10^{-23} \text{ m}^2 \text{ kg s}^{-2} \text{ K}^{-1}$ ,  $h$  is the Planck's constant with a value of  $6.6260 \times 10^{-34} \text{ m}^2 \text{ kg s}^{-1}$ ,  $e$  represents the charge of an electron and has a value of  $(1.602 \times 10^{-19} \text{ C})$  and  $m^*$  represents effective mass. Traditionally, this concept has been employed to determine how  $S$  changes as a function of  $n$ . Because eqn (5) indicates that electrical conductivity and charge carrier concentration are proportional to each other, a small charge carrier concentration results in a significant Seebeck coefficient with a lower  $\sigma$

$$\sigma = ne\mu, \quad (5)$$

where  $\mu$  is a symbol of the charge carrier's mobility. The trade-off between  $S$  and  $\sigma$  restricts the achievement of maximum PF. When the Seebeck coefficient and electrical conductivity are balanced, a maximum PF is produced, and for inorganic TE materials, this usually happens at carrier concentrations

ranging from  $10^{19}$  to  $10^{21} \text{ cm}^{-3}$ .<sup>5</sup> It has not yet been conclusively determined the best carrier concentration for organic compounds. OTE materials have a different conduction mechanism than traditional inorganic thermoelectric materials; therefore, the optimal carrier concentration may differ from that of inorganic materials.<sup>67</sup> Conductivity in conducting polymers and organic materials is usually induced by polaron hopping caused by the overlapping of the electron wave function on adjacent sites. When an electron moves down a chain while being trapped by a polarised field, lattice distortion may be created around the intense electron-phonon interactions. Compared to inorganic materials, which typically have carrier mobility in the range of  $1\text{--}10^3 \text{ cm}^2 \text{ V}^{-1} \text{ s}^{-1}$ , this method of electrical transport produces a charge carrier mobility of less than  $10^{-4}\text{--}10^1 \text{ cm}^2 \text{ V}^{-1} \text{ s}^{-1}$ .<sup>68</sup> The greatest power factor for organic materials then has a reasonably high carrier concentration.

**1.2.2. Thermal conductivity in organic materials.** One of the three important parameters for TE materials is thermal conductivity ( $k$ ), which can be explained by eqn (6):

$$\kappa = \kappa_e + \kappa_l. \quad (6)$$

In this equation, the symbols  $\kappa_l$  and  $\kappa_e$  denote lattice thermal conductivity and electronic thermal conductivity, respectively. Electrical and thermal conductivities are proportional to each other according to Wiedemann-Franz's law (WFL).<sup>69,70</sup> The Lorenz number ( $L$ ), which is normally equal to  $L = 2.4433 \times 10^{-8} \text{ WU}$ , is used in this equation. Many organic conductive polymers can be used as TE materials. Liu *et al.* reported that the Lorenz number is compatible with its standard Sommerfeld value and that the WFL is valid for poly(3,4-ethylene dioxythiophene) polystyrene sulphonate (PEDOT:PSS).<sup>71</sup> Salamon *et al.* discovered that WFL holds a similar Lorenz number to Tetra-thiafulvalene-Tetracyanoquinodimethane (TTF-TCNQ).<sup>72</sup> However, some researchers have hypothesised that owing to the different electrical transports driven by polarons, the Lorenz number may not be identified as the traditional Sommerfeld value.<sup>67</sup> The Lorenz number and Sommerfeld value may differ owing to the structure and level of doping.<sup>67,73,74</sup> The lattice thermal conductivity of materials caused by the transfer of energy by phonons is frequently used in eqn (7):

$$K_L = \frac{1}{3} C v l, \quad (7)$$

where  $v$  represents the sound velocity,  $l$  represents the phonon mean free path, and  $C$  represents the heat capacity. As per observations, the values of  $C$  and  $l$  for PEDOT:PSS are  $1.83 \times 10^{-6} \text{ J K m}^{-3}$  and  $0.1 \text{ nm}$ , respectively.<sup>75</sup> Organic materials frequently have sound velocities between  $10^3$  and  $10^4 \text{ ms}^{-1}$ . For example, the sound velocities of poly(3,4-ethylene dioxythiophene) polystyrene sulphonate (PEDOT:PSS) and poly(3-hexylthiophene)  $P_3\text{HT}$  materials are  $1.58$  and  $2.87 \text{ ms}^{-1}$ , respectively.<sup>76,77</sup> According to the literature estimate, the lattice thermal conductivities of PEDOT:PSS and  $P_3\text{HT}$  are  $0.3 \text{ W m}^{-1} \text{ K}^{-1}$  and  $0.5 \text{ W m}^{-1} \text{ K}^{-1}$ , respectively. These numbers fall within the established range ( $0.1\text{--}0.7 \text{ W m}^{-1} \text{ K}^{-1}$ ) for

thermal conductivities for various polymers.<sup>78,79</sup> Organic materials typically have the advantage of low thermal conductivity, which falls in the range of  $0.1\text{--}0.7 \text{ W m}^{-1} \text{ K}^{-1}$ , but the electrical conductivity of these materials is frequently low, *i.e.*,  $1 \text{ S cm}^{-1}$ .<sup>77-79</sup> In comparison, the lattice thermal and electrical conductivities of organic materials result in an order of magnitude.

The typical two-dimensional (2D) material is known as graphene,<sup>80-82</sup> which is made of a single layer of  $\text{sp}^2$  hybridised carbon atoms. It has been regarded as an extremely attractive choice for flexible thermoelectric (FTE) applications owing to its inherent advantages of being lightweight, non-toxic, flexible, and mechanically strong with great thermal stability.<sup>83</sup> Electrical transport with extremely high intrinsic carrier mobility<sup>84</sup> involves scalable synthesis in production, characteristics tuning by doping, and nanostructure defects that alter or functionalize thermoelectric properties.<sup>85</sup> The experimental power factors of graphene are  $6.93 \times 10^3$  and  $3.29 \times 10^3 \mu\text{W m}^{-1} \text{ K}^{-2}$  when p-type and n-type carriers are added to the graphene, respectively.<sup>86</sup> FTE materials are the most significant value ever recorded, with a PF as high as  $5.45 \times 10^3 \mu\text{W m}^{-1} \text{ K}^{-2}$ .<sup>87</sup> rGO nanosheets may offer a smooth function consistently at the previously unrecognised higher operating temperature of  $3000 \text{ K}$ . Additionally, some scientists<sup>88-93</sup> have already implemented these graphene-based thermoelectric materials into systems, such as generators,<sup>94</sup> supercapacitors,<sup>95</sup> cells,<sup>96</sup> and sensors<sup>97,98</sup> based on TE performance, among other things.

Several notable review papers on graphene-based thermoelectric hybrids have been published. Faruque *et al.*<sup>99</sup> briefly introduced the TE characteristics of graphene and various types of graphene-based thermoelectric hybrids. Graphene and its combinations have not been precisely described or given their precise optimisation processes. They are yet to be introduced for inclusion in gadgets. In recent years, Wang *et al.*<sup>100</sup> focused on graphene modification for fine-tuning its thermal, electrical, and TE properties.<sup>100</sup>

This article provides an overview of the material characteristics that influence the thermoelectric conversion efficiency of graphene. We discuss the theoretical elements and factors that influence these material properties and investigate challenges in applying graphene to thermoelectrics, unravelling the significance of graphene structural imperfection, nanostructure, and doping in addressing these problems.<sup>101</sup>

### 1.3 Graphene

**Thermoelectric properties of graphene.** We provide specific focus methods for increasing the TE characteristics of graphene. Because graphene is a semiconductor with a zero-band gap, it displays an ambipolar electric phenomenon. Mechanically exfoliated graphene has an RT carrier concentration of  $10^{13} \text{ cm}^2 \text{ V}^{-1} \text{ S}^{-1}$  and is near  $15\,000 \text{ cm}^2 \text{ V}^{-1} \text{ S}^{-1}$ . This allows for continuous switching of the charge carriers between holes and electrons.<sup>102,103</sup> An extremely high  $\mu$  performs well with high conductivity. Therefore, owing to its gapless nature, graphene typically has an  $S$  below  $100 \mu\text{V K}^{-1}$ .<sup>104,105</sup>



Experimentally, the  $ZT$  of pure graphene ranges from  $10^{-4}$  to  $10^{-3}$  owing to its incredibly high thermal conductivity and low Seebeck coefficient.<sup>106</sup> Even though implementing graphene in thermoelectric energy conversion seems difficult, several research efforts have achieved noticeable advancements.<sup>107,108</sup> In addition to grain refinement, the experiment conducted by Li *et al.*<sup>85</sup> with nano structuring revealed that the figure of merit of graphene may be enhanced up to 0.1, two to four orders of magnitude greater than pure graphene. However, more theoretical studies have also shown that it is feasible to increase the figure of merit of graphene above unit 1, making it equivalent to cutting-edge TE materials.<sup>109–111</sup> Consequently, graphene has been a promising alternative for applications that depend on its effects. These polymer composites take advantage of the low  $k$  of polymers and the high  $\sigma$  of graphene. Consequently, thermoelectric performance is enhanced by the interaction of polymers and graphene.<sup>101</sup>

Graphene has garnered significant attention from various fields, including chemistry, physics, and materials science. The growing interest in the TE application of graphene has resulted in a significant amount of work and rapid progression of research, necessitating a timely review of previous studies in this field. Graphene-derived composites are carbon-based materials, and the incorporation of graphene into composites can contribute to environmentally friendly TE solutions compared to traditional materials that may contain toxic elements. Better charge carrier mobility is made possible by the high electrical conductivity of graphene-derived composites, which is crucial for optimising TE performance. Graphene has a large surface area, providing different sites for interaction with other materials in composite films. Because of their flexibility and light weight, graphene-derived composites are a good choice for TE devices that are portable and adaptable. Large-scale TE applications are becoming increasingly viable owing to the advancement of graphene fabrication processes and the increased scalability of composites generated from graphene. Enhanced Seebeck coefficients in graphene-derived composites can lead to higher TE efficiency due to the distinct electrical structure of graphene. This comprehensive review aims to provide an overview of the TE properties and optimisation strategies employed in graphene and graphene-based composites. Several justifications exist for the recognition of graphene-derived composites as highly promising materials for TE applications. The mechanical strength and flexibility of graphene are well known. Composites may be used for strong and flexible TE applications because graphene provides mechanical stability and longevity. Graphene is a 2D material that provides low-dimensional effects on composite materials. These effects have the potential to improve TE properties, specifically by increasing the density of electronic states. This enhancement is favourable for the improvement of  $ZT$ . However, current investigations are primarily directed towards augmenting their efficiency, and scalability, and understanding their stability to facilitate their practical integration into energy harvesting and waste heat recovery systems.

**1.3.1. Nanostructured graphene.** A graphene nanoribbon (GNR) is a quasi-one-dimensional (1D) structure formed by selectively patterning graphene in a specific direction. A graphene nanoribbon (GNR) with a width of 130 can be structured to exhibit either zigzag edges (ZGNR) or armchair edges (AGNR). ZGNR exhibits metallic characteristics. In contrast, the AGNR demonstrates behaviour typical of a metal or semiconductor, with a band gap that inversely correlates with its width.<sup>112,113</sup>

**1.3.2. Graphene doping.** By altering phonon dispersion and introducing isotope scattering, thermal conduction may be limited by isotope effects.<sup>114,115</sup> In both armchair and zig-zag directions, while preserving the same atomic and electrical structure, they can be reduced by up to 80%<sup>116</sup> by employing some  $^{12}\text{CH}_4$  as carbon compounds and replacing  $^{12}\text{C}$  with  $^{13}\text{C}$  in chemical vapour deposition (CVD) graphene. Remarkable electrical properties of graphene are still present because the electrical structure of  $^{13}\text{C}$  mostly resembles that of  $^{12}\text{C}$ .

**1.3.3. Boundary defect and structural defect in graphene.** A structural imperfection, such as a vacancy, an interstitial, a substitution, or a line defect, breaks the chemical bond between neighbouring atoms.<sup>115</sup> Graphene with  $\text{sp}^2$  hybridization and an energy of 5.9 eV is the strongest bond in nature<sup>117</sup> and leads to high defect formation energy, which results in experimental samples having a lower defect concentration. The sample is nonetheless susceptible to various imperfections owing to the varied production methods for graphene. Reduced thermal conductivity is the result of any irregularity or impurities in the graphene matrix, which increases phonon scattering.<sup>118</sup>

In their study, Huang *et al.* investigated two compounds: (aromatic-dicyanovinyl)dipyrrolo[3,4-*c*]pyrrole-1,4-diylidene)-bis(thieno[3,2-*b*]thiophene) (referred to as A-DCV-DPTT) and (quinoid-dicyano-methylene-dipyrrole-1,4-diylidene)bis(thieno[3,2-*b*]thiophene) (referred to as Q-DCM-DPPT). The compounds exhibited a notable Seebeck coefficient value of n-type ( $-1000 \mu\text{V K}^{-1}$ ). The Seebeck coefficient value of n-type ( $-1215 \mu\text{V K}^{-1}$ ) was obtained for A-DCV-DPPTT in the absence of a dopant.<sup>119</sup> Kanahashi *et al.* successfully conducted experimental research to achieve remarkably high PFs of  $6.93 \times 10^3$  and  $3.29 \times 10^3 \mu\text{W m}^{-1} \text{K}^{-2}$  through p- and n-type doping in graphene, respectively. The pristine state of CNT Bis was characterised by their p-type behaviour, which can be attributed to the dominance of holes as the primary charge carriers. Following the introduction of a doping treatment, it is observed that the Fermi level undergoes an upward shift towards the conduction band of the CNT. This phenomenon can be attributed to the charge transfer interaction occurring between the CNT and the introduced dopants. Consequently, the Fermi level undergoes a shift towards the conduction band, leading to the transformation of p-type CNTs into n-type CNTs. This shift ultimately decreases electrical conductivity.<sup>120</sup> In their study, David *et al.*<sup>121</sup> introduced an innovative technique for the fabrication of CNT-based polymer composites using a spray doping method. This approach enables the facile influence of the TE properties on the resulting materials. The fabrication



**Table 1** Summary of the synthesis method and thermoelectric performance at room temperature of some common organic materials with graphene

| Hybrid                                           | Synthesis                            | $\sigma$<br>(S cm <sup>-1</sup> ) | $S$<br>( $\mu$ V K <sup>-1</sup> ) | PF<br>( $\mu$ W m <sup>-1</sup> K <sup>-2</sup> ) | $K$<br>(W m <sup>-1</sup> K <sup>-1</sup> ) | $ZT$    | Ref. |
|--------------------------------------------------|--------------------------------------|-----------------------------------|------------------------------------|---------------------------------------------------|---------------------------------------------|---------|------|
| PANi/graphene                                    | Solution dispersion                  | 856                               | 15                                 | 19                                                | —                                           | —       | 123  |
| PANi/rGO                                         | <i>In situ</i> polymerisation        | 3677                              | 24                                 | 214                                               | —                                           | —       | 124  |
| PANi/graphene/PANi/DWNT                          | Layer-by-layer deposition            | 1080                              | 130                                | 1825                                              | —                                           | —       | 55   |
| PANi/graphene-PEDOT:PSS/<br>PANi/DWNT-PEDOT; PSS | Layer by layer deposition            | 1900                              | 120                                | 2710                                              | —                                           | —       | 61   |
| SWCNT/PEDOT:PSS DMSO, GA                         | Oxidative chemical polymerisation    | 400                               | 0.4                                | 25                                                | 0.4                                         | 0.02    | 53   |
| CNT/PVAc                                         | Solution method                      | 48                                | 45                                 | —                                                 | 0.34                                        | 0.006   | 125  |
| PANi/graphene nanosheets<br>mechanical blending  | Spin coating and mechanical blending | 123                               | 34                                 | —                                                 | —                                           | —       | 126  |
| PEDOT:PSS/graphene fullerene                     | Mixing                               | 700                               | 25                                 | —                                                 | 0.4                                         | 0.06    | 127  |
| PEDOT:PSS/graphene (100:1)                       | <i>In situ</i> polymerisation        | 1469                              | 46.9                               | 3.23                                              | 0.19                                        | 0.00046 | 128  |
| PEDOT:PSS/graphene (100:2)                       | <i>In situ</i> polymerisation        | 3200                              | 59                                 | 11.09                                             | 0.14                                        | 0.021   | 128  |

process of p-type TE composites comprising CNTs and PVDF involved the utilisation of a drop casting method. Subsequently, the film underwent a doping process in which polyethyleneimine (PEI), a small molecule n-type dopant, was introduced. This doping procedure was carried out using a 3D-printed thermoplastic stencil mask. The objective of this process was to achieve a conversion from p-type to n-type within the film. The experiment findings indicate that a rapid conversion from p-type to n-type was observed when the mass ratio of PEI to CNT ranged from 0 to 0.2. Additionally, it was observed that the Seebeck coefficient reached its highest value of  $-32 \mu\text{V K}^{-1}$ . In their study, Bharti *et al.*<sup>122</sup> presented a remarkable observation regarding the conduction behaviour of FeCl<sub>3</sub>-doped free standing poly(3-hexylthiophene) (P<sub>3</sub>HT) films. The findings reveal a significant departure from conventional p-type conduction to n-type conduction, which can be attributed to the influence of ionic transport. The phenomenon of thermodiffusion in the observation of a large n-type Seebeck coefficient is approximately  $-2.7 \mu\text{V K}^{-1}$ , along with a relatively high electrical conductivity of approximately  $1 \text{ S cm}^{-1}$ .

## 2. Discussion of OTE materials based on graphite and its composites

Graphene is a newly emerging 2-D crystalline carbon compound with extremely excellent electrical properties and sufficient TE performance. The organic TE materials recently produced include GO, rGO, and graphene nanosheets, and their fabrication processes, along with potential applications, are discussed here.

### 2.1 Graphene + organic thermoelectric materials

Organic materials, especially conductive polymer materials, are inexpensive, lightweight, highly flexible, easy to fabricate, and have very low thermal conductivity, making them particularly promising thermoelectric materials. Conjugated polymers have been identified as the most extensively researched polymer thermoelectric materials. These include PEDOT:PSS poly(3,4-ethylene dioxythiophene) polystyrene sulphonate, polypyrrole (Py), polyacetylene (PA), polyaniline (PANi), and poly(3-hexylthiophene) (P<sub>3</sub>HT). However, these organic conductive

materials have some demerits because of their poor electrical transport properties compared to traditional inorganic materials. Graphene is preferred as a doping hybridised with conductive conjugated polymers to improve electron transport properties owing to its good mechanical properties, prosperous electronic state, large surface area, high flexibility, high mobility, and low density. Table 1 shows the synthesis method and the properties of the graphene and conductive polymers.

The polymers frequently employed in thermoelectric applications encompass poly(3,4-ethylene dioxythiophene) poly(styrene sulfonate) (PEDOT:PSS), polyaniline (PANi), polyvinyl acetate (PVAc), polyacetylene, poly(3-hexyl thiophene) (P<sub>3</sub>HT), polypyrrole (PPy), and poly(2,7-carbazolynevinylene). In their study, Zhang *et al.*<sup>129</sup> incorporated fullerene-decorated reduced graphene oxide (rGO) into PEDOT:PSS. Functionalisation was accomplished through p-p stacking at the liquid-liquid interface. The electrical conductivity of the nanohybrid filler was enhanced by a factor of 7, resulting in a value of  $70\,000 \text{ S m}^{-1}$ . Additionally, the thermopower experienced a 4-fold increase. The thermal conductivity also improved from  $0.2$  to  $2 \text{ W m}^{-1} \text{ K}^{-1}$ . These enhancements led to the attainment of a  $ZT$  value of 0.067 when the nanohybrid was composed of 30 wt% and had an rGO-fullerene ratio of 7:3. The improvement in TE properties was attributed to the presence of interfacial phonon scattering and energy filtering. PEDOT:PSS-rGO composite film fabrication has been achieved by utilising the solution spin coating method.<sup>130</sup> The addition of 2 wt% of reduced graphene oxide enhances the power factor of the composite materials, increasing PF from  $2.03$  to  $11.09 \mu\text{W m}^{-1} \text{ K}^{-2}$ . Simultaneously, the thermal conductivity of the composite material decreases from  $0.24$  to  $0.14 \text{ W m}^{-1} \text{ K}^{-1}$ . The  $ZT$  value is increased by a factor of 10, resulting in a matter of 0.021. The observed increase in PF can be attributed to the robust p-p interactions between rGO and PEDOT:PSS open rings, which facilitate efficient charge transfer within the composite material. The low thermal conductivity of the composite can be attributed to its multilayer porous structure, which serves as a phonon scattering centre. The preparation of highly conductive composites based on PEDOT:PSS-rGO was carried out through *in situ* polymerisation, as conducted by Yoo's group.<sup>131</sup> The composites exhibited increased electrical conductivity ranging from  $453$  to  $637 \text{ S m}^{-1}$ .





at a concentration of 3 wt% of rGO. Additionally, the PF showed improvement, increasing from 24.17 to 45.68  $\mu\text{W m}^{-1} \text{K}^{-2}$ . The enhanced electrical conductivity of the composites can be attributed to the existence of well-organised and structured rGO sheets. These sheets facilitate the arrangement of PEDOT:PSS molecules into morphologies that promote efficient charge transport. PANi-graphene nanoplatelet (GNP) nanocomposites were synthesised through the *in situ* polymerisation of aniline monomer in the presence of GNP.<sup>132</sup> The thermal expansion coefficient (TEP) of the nanocomposites was influenced by both the concentration of aniline and the protonation of polyaniline (PANi). TEP values reaching up to 33  $\mu\text{V K}^{-1}$  were attained when the weight percentage of PANi was 40% and the protonation ratio was 0.2. The electrical conductivity is enhanced to 59  $\text{S m}^{-1}$ , leading to a ZT value that surpasses both PANi and GNPs by two orders of magnitude. The incorporation of graphene nanoplatelets (GNP) into the composite material resulted in the elongation of the polymeric chains of polyaniline (PANi). This elongation led to an increase in the mobility of the charge carriers, thereby improving the PF. The presence of GNP also contributed to the reduction of thermal conductivity in the composite material. Other authors have also made similar observations regarding the thermal and electrical properties of PANi/graphene composites.<sup>133</sup> PVAc/graphene-iron oxide (GINC) and PVAc-graphene nanocomposites were fabricated through a two-step process involving ultrasonication and subsequent hot compaction. The PVAc-GINC composite demonstrated an optimal electrical conductivity of  $2.18 \times 10^4 \text{ S m}^{-1}$  and a thermoelectric power (TEP) value of 38  $\mu\text{V K}^{-1}$  by adjusting the concentrations of GINC and graphene. The PF value of this composite material was measured to be 32.90  $\mu\text{W m}^{-1} \text{K}^{-2}$ , which is 27 times higher than that of the PVAc-graphene composite. The thermal conductivity value was also determined to be 3.21  $\text{W m}^{-1} \text{K}^{-1}$ , resulting in a ZT value of 0.0031. The GINC filler enhanced the electrical conductivity and thermoelectric power (TEP) of the nanocomposites. However, the presence of iron oxide decorated on graphene disrupted the thermally conductive network. Consequently, the overall thermoelectric properties of the nanocomposites improved.

### 2.1.1. Synthesis method for graphene with conductive polymer composites

**Solution dispersion.** They prepared a solution of PANi with graphene using the solution dispersion method, and it exhibits  $\sigma$  of 856  $\text{S cm}^{-1}$  and a PF of 19  $\mu\text{W m}^{-1} \text{K}^{-2}$  because graphene has outstanding electrical properties and a strong  $\pi$ - $\pi$  conjugated bond with PANi and graphene.<sup>123</sup> Although graphene agglomeration is unavailable at high filler content, it still limits the degree of uniformity owing to the solution dispersion method. The prevention of graphene aggregation remains an essential issue in the solution dispersion method.

**Powder mixing method.** Ceramic powder mixing process for conductive polymers and graphene. Graphene and organic conductive polymers are mixed mechanically, often by ball milling, to obtain uniform dispersion before being heated or cold pressed into a pellet or foil.<sup>126</sup> Powder mixing can scarcely achieve uniform distribution because the as-prepared graphene or polymer can easily agglomerate.

**Layer-by-layer deposition.** By repeatedly exposing a hybrid film to a solution comprising cationic and anionic components, layer-by-layer deposition allows the production of nanoscale films with an arranged layer-by-layer stacking structure.<sup>134</sup> Cho *et al.* prepared an organised molecular structure of PANi/graphene/PANi/DWNT hybrid with an ordered molecular structure.<sup>55</sup> DWNT and graphene are negatively charged in this case, while PANi is positively charged. A neighbouring layer with a reverse charge can spontaneously produce a structural arrangement. An increase in the number of deposition cycles improves the Seebeck coefficient and electrical conductivity. A PF of 1825  $\mu\text{W m}^{-1} \text{K}^{-2}$  was obtained. In a recent study,<sup>61</sup> graphene and DWNT were stabilised using PEDOT:PSS, producing a thin film of PANi/graphene-PEDOT:PSS/PANi/DWNT-PEDOT:PSS hybrids, which were also manufactured by the layer-by-layer (LBL) process. Fig. 7 shows that a quad-layer of PANi/graphene-PEDOT:PSS was created through a series of depositions. A quad layer was produced. You can obtain the required layer thickness by repeating the sequence. The modified film showed an enhanced electrical

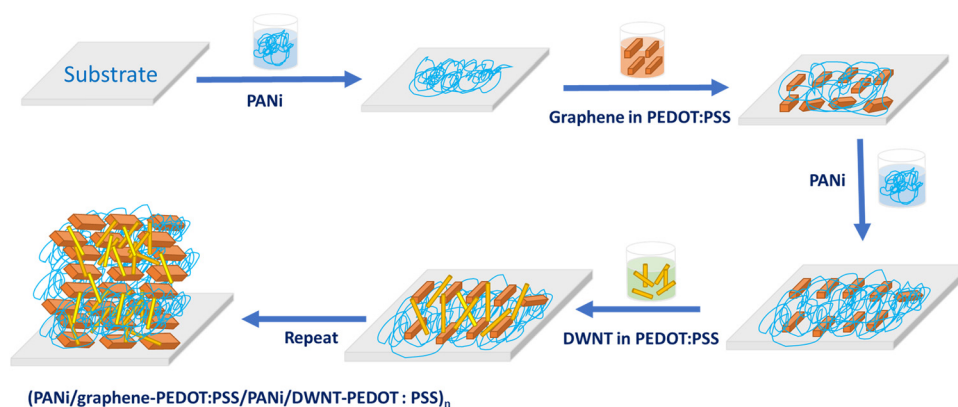


Fig. 7 Layer-by-layer deposition method of PANi/graphene-PEDOT:PSS/PANi/DWNTs-PEDOT:PSS hybrids.

conductivity of  $1900 \text{ S cm}^{-1}$  and a record maximum power factor of  $2710 \mu\text{W m}^{-1} \text{ K}^{-2}$ . This is comparable to the traditional inorganic thermoelectric material  $\text{Bi}_2\text{Te}_3$ , which has the best RT thermoelectric properties. The LBL method provides an opportunity to prepare various organic materials with graphene rods with increased power factor expectations.

Zhang *et al.*<sup>135</sup> developed a multipurpose superelastic thermoelectric sponge based on graphene, which has a high  $S$  and a maximum compressive strain of  $49.23 \text{ mV K}^{-1}$ , or 98%. The sponge maintains good mechanical and thermoelectric stability, and the Seebeck retention coefficient stays at 92.5% after 10 000 compression cycles with 30% elongation. A  $4 \times 4$  array TE device is placed on top of the working CPU temperature by 8 K, offering a workable method for continuously generating power and thermal management. Du *et al.*<sup>93</sup> fabricated a composite made of graphene nanosheets and PANi, and they reported a high PF of  $5.6 \mu\text{W m}^{-1} \text{ K}^{-2}$  because these composites have high charge carrier mobility. Using another combination of graphene, fullerene ( $\text{C}_{60}$ ), and PEDOT:PSS, Wang *et al.*<sup>136</sup> obtained a higher PF and figure of merit ( $32 \mu\text{W m}^{-1} \text{ K}^{-2}$  and a  $ZT$  value of 0.067) at RT. A layer-by-layer synthesis of stabilised CNTs, graphene, and PANi is a different method that uses graphene. This method displays a power factor of  $1825 \mu\text{W m}^{-1} \text{ K}^{-2}$  at 300 K.<sup>137</sup>

Kim *et al.*<sup>138</sup> prepared composite films containing 1, 2 and 3 wt% graphene with PEDOT:PSS *via* the spin coating. Analysis using Raman and X-ray photoelectron microscopy shows the presence of strong interactions that assisted in the dispersed solution of graphene and PEDOT:PSS. Compared with CNT based on identical weight, the interfacial area increased 2–10 times by the evenly distributed graphene. A thin film of PEDOT:PSS with a PF of  $11.09 \mu\text{W m}^{-1} \text{ K}^{-2}$  and  $ZT$  of 0.02 contained two wt% graphene. Du *et al.*<sup>93</sup> report for the first time a trend of increased Seebeck coefficient and  $\sigma$  with increasing GN concentration (up to a 1:1 ratio) in PANi-GNs composites.

The ratios used to create the four different compositions were PANi-GNs 4:1, 3:1, 2:1, and 1:1. The maximum values of  $S$  and  $\sigma$  were observed at a 1:1 concentration of PANi-GNs. The observed phenomenon can be attributed to the significant increase in carrier mobility. Adding 50 wt% of graphene nanosheets (GNs) increased the pellets and thin film. In particular, the PF of the pellet increased from 0.64 to  $5.6 \mu\text{W m}^{-1} \text{ K}^{-2}$ , while the PF of the thin film increased from 0.05 to  $1.47 \mu\text{W m}^{-1} \text{ K}^{-2}$ . Similarly, Xiang *et al.*<sup>139</sup> manufactured PANi-graphene composites *via in situ* aniline monomer polymerisation with graphene nanoplatelets (GNP). The intense interaction between GNP and PANi produced a homogeneous coating of GNs. The authors created a composite that resembles the paper. The  $S$  of the synthesised composite varies with the quantities of polyaniline and the initial amount of aniline concentration in the mixture. With a protonation ratio of 0.2 and a composite containing 40 wt% PANi, its value increases to  $33 \mu\text{V K}^{-1}$ . The addition of GNP boosts the  $\sigma$  of the composite to  $559 \text{ S cm}^{-1}$ . It was discovered that the  $ZT$  value was two orders of magnitude higher than that of PANi or

graphene. The TE efficiency of PEDOT:PSS can be improved by carbon nanotubes. It was shown in the literature,<sup>138–143</sup> that increasing graphene content by 2–3 wt% caused  $ZT$  to increase ten times. Comparing this value to carbon nanotube (CNT)-based composites, it is significantly greater. Strong  $\pi$ - $\pi$  interaction with help from more distribution is the cause. Raman spectroscopy lends support to these connections. Compared to CNT with a similar weight, the contact area is increased by 2–10 times when graphene is dispersed evenly. The higher carrier mobility of graphene increases the electrical conductivity, but the decreased thermal conductivity of graphene/PEDOT:PSS is greater than that of the pure PEDOT:PSS thin film, which contains 35 wt% of SWCNT.<sup>14</sup> The author provided a comprehensive explanation for this anomaly of the two attributes. First, a clearly explained porous multi-layer structure serves as a phonon dispersion centre, and second, phonons predominate in the thermal conductivity of such materials. Lattice thermal conductivity ( $k_l$ ) has a more significant influence than electronic thermal conductivity ( $k_e$ ); the combination of PEDOT:PSS and two wt% graphene showed the highest  $ZT$  value of  $2.1 \times 10^{-2}$  at 300 K. Compared to pure PEDOT:PSS, this value was ten times greater. A practical and innovative technique for improving TE efficiency is fabricating a composite by adding graphene to PEDOT:PSS. Additionally, Yoo *et al.*<sup>144</sup> developed a composite made of PEDOT:PSS with graphene and investigated its potential application in waste heat energy recovery. Higher Seebeck and power factors are displayed by the composite that contains three wt% graphene.

## 2.2 Graphene+ inorganic thermoelectric materials

Graphene and CNTs have excellent mechanical stability, high conductivity, and significant charge carrier mobility<sup>145,146</sup> and are most prominently used in inorganic thermoelectric composites.<sup>147–153</sup> Dong *et al.*<sup>147</sup> prepared nanocomposites of PbTe/graphene using a wet chemical method. The powder was prepared using the spark plasma sintering method at 580 K, and a  $ZT$  of the obtained product, which is 0.7 at 670 K, was reported. For graphene composite materials, PbTe has a mass ratio of 5%. A  $\text{Bi}_2\text{Te}_3$  nanowire (NW)/graphene composite film was prepared using the wet chemical method, followed by the sintering method at 300 K.<sup>148</sup> The composite film contained 20 wt% of  $\text{Bi}_2\text{Te}_3$ , and a  $ZT$  value of 0.2 was obtained.

Graphene materials with  $\text{Bi}_2\text{Te}_3$  were prepared *via* a hydrothermal process, followed by a spark plasma sintering process, and the  $ZT$  of the composite material containing 0.2% graphene at 475 K was 0.21.<sup>154</sup> In the work by Wang *et al.*,<sup>155</sup> rather than simply aiming for high performance, they attempted to develop flexible thermoelectric composites based on abundant, inexpensive or environmentally friendly inorganic thermoelectric materials. Because n-type flexible thermoelectrical materials are highly desirable, most inorganic materials used in flexible thermoelectric composites so far are made up of rare or hazardous elements, so abundant and inexpensive non-toxic Zn-doped pyrite  $\text{Cu}_{1-x}\text{Zn}_x\text{FeS}_2$  ( $x$  is 0.01, 0.02, 0.03) flexible PEDOT:PSS with graphene electrical networking is an essential candidate for n-type flexible thermoelectric films. The



characterisation of hybrid films, which are designed using a combination of binary and ternary  $\text{Cu}_{1-x}\text{Zn}_x\text{FeS}_2/\text{PEDOT:PSS}$  and  $\text{Cu}_{0.98}\text{Zn}_{0.02}\text{FeS}_2/\text{PEDOT:PSS}/\text{graphene}$ , is performed. The  $\sigma$  of the ternary film is four times greater than that of the binary film, with a maximum power factor of approximately  $23.7 \mu\text{W m}^{-1} \text{K}^{-2}$ . The optimal ternary film can retain more than 80% of  $\sigma$  even after 2000 cycles of bending and exhibits extraordinary flexibility owing to the network made of PEDOT:PSS and graphene. A prototype thermoelectric device with five legs constructed of optimal foil produced a voltage of 4.8 mV at  $\Delta T$  and 286 K. The development of low-cost chalcopyrite-based composite films with high flexibility shows the potential for cost-sensitive flexible thermoelectric (FTE) applications. Paris *et al.*<sup>156</sup> developed foldable and transparent generators and storage devices (AC < 1 mm thick) with an active layer (AC) thickness of approximately 20 nm piezoelectric between two graphene monolayers. They were manufactured by sandwiching the material and the solid electrolyte, respectively. A portable photoresistor with a thickness of 30 nm (AC-30) was created by combining a single layer of graphene with a fragile layer of ZnO deposited onto a PET or ITO substrate. Piezoelectric nanogenerators typically showed steady peak voltages of 5.5 V and a power density of  $0.2 \text{ nA cm}^{-2}$ . Finally, the portable photoresistor prepared in this way exhibited an adequate reaction to visible light, producing a high (in mA, even at low bias potentials) and an on/off current ratio of 1.8. The cold pressing process prepared Agarwal *et al.*<sup>123</sup> bulk  $\text{Bi}_2\text{Te}_3$  and graphene materials, and the  $ZT$  of the composite graphene material containing 0.05 wt% at 402 K was 0.92. Liang *et al.*<sup>154</sup> synthesised  $\text{Bi}_2\text{Te}_3$  and graphene composites *via* hydrothermal synthesis combined with spark plasma sintering. A  $\text{Bi}_2\text{Te}_3$  particle was coated with 30–200 nm-sized graphene nanosheets in the precursor nanopowder. At 475 K, the maximum value of  $ZT$  was 0.21, achieved with a graphene content of 0.2 vol%, which is 31% higher than pure  $\text{Bi}_2\text{Te}_3$  material. Gobpant *et al.*<sup>157</sup> developed SnTe-based powders using a hybrid microwave solid-state process, including SnTe,  $\text{Sn}_{0.95}\text{Bi}_{0.05}\text{Te}$ , and SnTe, with graphene addition. At 325 K, the SnTe with five wt% graphene demonstrated a reasonable PF, and the thermal conductivity decreased from  $10 \mu\text{W m}^{-1} \text{K}^{-2}$  for SnTe to  $2 \mu\text{W m}^{-1} \text{K}^{-2}$ . The dimensionless parameter  $ZT$  of SnTe was increased from 0.07 to 0.35 with five wt% graphene, a 5-fold increase. Dong *et al.*<sup>147</sup> synthesised PbTe and graphene nanocomposites *via* an efficient and innovative wet chemical process. PbTe/graphene nanocomposites achieve a  $ZT$  value of 0.7 at 670 K, which is a substantially more incredible value. This has a considerably higher  $ZT$  than any n-type PbTe

synthesised using a conventional methodology, and it is six times greater than the pure PbTe sample.

### 2.3 rGO + organic composite

Ube *et al.*<sup>124</sup> recently created a camphor sulfonic acid (CSA) filled with rGO and PANi film fabricated *via* an *in situ* polymerisation process using an adequately insulated heat rGO. The  $\sigma$  of this composite film is very high at  $3677 \text{ S cm}^{-1}$ , so the competing PF is  $214 \mu\text{W m}^{-1} \text{K}^{-2}$ . *In situ* polymerisation may provide a more equal distribution than solution dispersal or powder mixing. Wang *et al.*<sup>158</sup> reported that cryogenic milling uniformly combined PANi and rGO uniformly, and spark plasma sintering was used to make them more challenging. rGO/PANi hybrid composites have significantly better TE characteristics than pristine bulk PANi composites. Surprisingly, the maxima of  $S$  and  $\sigma$  are  $15.934 \mu\text{V K}^{-1}$  and  $1858.775 \text{ S m}^{-1}$ , respectively, and the highest  $ZT$  value of the rGO/PANi hybrid composite was 0.00042.

Xina<sup>159</sup> reported that the PF of the film reached up to  $7.28 \mu\text{W m}^{-1} \text{K}^{-2}$ , which is significantly greater than that of a pristine polypropylene nanotube. Practical vacuum filtering and HI treatment were used to create a free-standing, foldable polypropylene nanostructure hybrid film successfully. Graphene nanosheet agglomeration was prevented, and conductive channels were produced by the hybrid film's polypropylene nanotube/rGO-linked structure. Ali *et al.*<sup>160</sup> studied the PANi/doped reduced graphene oxide nanomaterials synthesised using wet chemical polymerisation combined with the hydrothermal method. The nanocomposites with only one wt% of the SNrGO had a Seebeck coefficient of  $-1.75 \mu\text{V K}^{-1}$ , which is an n-type thermoelectric material, with good  $\sigma$  and intrinsic deficient  $k$  reported as  $31 \text{ S m}^{-1}$  and  $0.51 \mu\text{W m}^{-1} \text{K}^{-1}$ , respectively, resulting in a  $95 \mu\text{W m}^{-1} \text{K}^{-2}$  PF with a  $ZT$  of 0.05 at RT. Similarly, Xu *et al.*<sup>161</sup> synthesised a nanocomposite made of PEDOT-rGO with significantly improved thermoelectric properties. The thermoelectric performance of a nanocomposite produced by template-directed *in situ* polymerisation was considerably enhanced at ambient temperature with a PF 13.3 times greater than that of PEDOT at  $5.2 \pm 0.9 \times 10^{-6} \mu\text{W m}^{-1} \text{K}^{-2}$ .

### 2.4 rGO + Inorganic composite

Du *et al.*<sup>146</sup> prepared a nanocomposite of rGO/ $\text{Bi}_2\text{Te}_3$  bulk material manufactured using a hot pressing method. The  $\sigma$  of these nanocomposite materials decreased as the measured temperature increased from 298 K to 573 K. However, the exact value of  $S$  first increased and then decreased. Consequently,

**Table 2** Summary of the synthesis method and thermoelectric performance at room temperature of common inorganic materials with graphene

| Material                                                                                        | Synthesis              | $\sigma$ ( $\text{S cm}^{-1}$ ) | $K$ ( $\text{W m}^{-1} \text{K}^{-1}$ ) | $S$ ( $\mu\text{V K}^{-1}$ ) | $ZT$ | Ref.        |
|-------------------------------------------------------------------------------------------------|------------------------|---------------------------------|-----------------------------------------|------------------------------|------|-------------|
| $\text{Bi}_2\text{Te}_3/0.25\%$ rGO                                                             | Hot-pressing method    | $8 \times 10^{-6}$              | 1.3                                     | −80                          | —    | 146         |
| $\text{Bi}_2\text{Te}_3/\text{graphene}$                                                        | Hydrothermal SPS       | $1.05 \times 10^{-5}$           | 2.5                                     | −113                         | 0.21 | 154 and 164 |
| $\text{Bi}_2\text{Te}_3/\text{graphene}$                                                        | Wet chemical sintering | $3.5 \times 10^{-5}$            | 0.7                                     | −132                         | 0.2  | 148         |
| $(\text{Bi}_{0.98}\text{In}_{0.02})_2\text{Te}_{2.7}\text{Se}_{0.3}/\text{wt}\%$ rGO composites | Solid-state reaction   | $3.0 \times 10^{-3}$            | 0.8                                     | −140                         |      | 162         |
| PEDOT:PSS/ $\text{Bi}_2\text{Te}_3$                                                             | Ball milled            | 250                             | 0.55                                    | 150                          | 0.08 | 165         |



the PF of the bulk material increased first and then decreased. At 423 K, a nanohybrid base material containing 0.25 wt% rGO had a PF of  $1340 \mu\text{W m}^{-1} \text{K}^{-2}$ . Similarly, Kumar *et al.*<sup>150</sup> synthesized the nanocomposites of  $\text{Bi}_2\text{Te}_3/\text{rGO}$  via the refluxing technique and then obtained nanocomposites pressed into pellets. The  $ZT$  value of the pellet at  $\sim 340 \text{ K}$  was  $\sim 0.35$ . Table 2 shows graphene's synthesis method and properties with their derivative and inorganic thermoelectric materials.

Hegde *et al.*<sup>162</sup> reported the TE efficiency of pure  $(\text{Bi}_{0.98}\text{In}_{0.02})_2\text{Te}_{2.7}\text{Se}_{0.3}$  with rGO composite in the temperature range of 10–325 K. These compounds follow the rhombohedral structure of the space group  $R_3m$ . The presence of 0.02 wt% rGO in the matrix of  $(\text{Bi}_{0.98}\text{In}_{0.02})_2\text{Te}_{2.7}\text{Se}_{0.3}$  reduced thermal conductivity by 1.6-fold and electrical resistance by 10-fold at 325 K  $(\text{Bi}_{0.98}\text{In}_{0.02})_2\text{Te}_{2.7}\text{Se}_{0.3}/\text{rGO}$  because of the interaction between interfacial dispersion and antistite defects. At 325 K, the maximum PF of  $7 \mu\text{W m}^{-1} \text{K}^{-2}$  and the figure of merit of 0.0026 were obtained with the  $(\text{Bi}_{0.98}\text{In}_{0.02})_2\text{Te}_{2.7}\text{Se}_{0.3}$  containing 0.01 wt % rGO. At low temperatures, its TE cooling applications may result from properly optimising the  $(\text{Bi}_{0.98}\text{In}_{0.02})_2\text{Te}_{2.7}\text{Se}_{0.3}$  containing 0.02 wt % rGO. Kim *et al.*<sup>163</sup> prepared bulk nanocomposites using  $\text{Mg}_{1.96}\text{Al}_{0.04}\text{Si}_{0.97}\text{Bi}_{0.03}$  and a few layers of rGO through an ultrasonic-based wet chemical pulverising mixing method to enhance the thermoelectric performance and mechanical stability. Surprisingly, a high  $K_{\text{IC}}$  of 1.88 MPa  $\text{m}^{1/2}$  was achieved with rGO 3 vol%, and an excellent  $ZT$  value of 0.6 was observed.

## 2.5 C derivatives (CNT, etc.) + organic/inorganic composite

Because of their exceptional electrical characteristics, carbon nanotubes have been regarded as viable options for various applications, such as touch screens, field emission displays, solar cells, and field effect transistors. The  $\sigma$  of these materials is greater than that of the other polymer composites. They use another dopant because carbon nanotubes are also used as fillers in polymer composites. A study of TE materials has been more interesting with carbon nanotubes. Owing to their dimensional structure, it has been reported that 1- or 2-dimensional thermoelectric materials have lower dimensions than bulk materials and can sometimes perform better. By increasing the density of the state near the Fermi energy and reducing the sizes, CNT can increase  $S$ .<sup>166</sup>

Kim *et al.*<sup>167</sup> used polyethyleneimine,  $\text{NaBH}_4$ , and diethylenetriamine to treat CNT to create n-type materials with  $S = 86 \mu\text{V K}^{-1}$  and  $\sigma = 52 \text{ S cm}^{-1}$ . A flexible TEG made from 72 CNT foil thermocouples (Fig. 7) with a 49 K temperature gradient yielded an open circuit voltage of 465 mV. Additionally, multi-walled TE fabrics are manufactured by Hewitt *et al.*<sup>168</sup> using p-type and n-type CNT/PVDF composite films, and the sum of the thermoelectric power produced by these textiles is calculated and found to be contributed from each p-type and n-type layer. At 50 K, the thermoelectric fabric with 72 film layers had a maximum output of 137 mW. Fig. 7 is connected to type 1, a device that can recycle the temperature gradient that runs parallel to the TEG surface. This is the fundamental distinction between commercially available inorganic TE generators (attached to a  $\pi$ -shaped structure). This is because the  $\pi$ -type

inorganic TEG may recycle the surface average temperature difference of the n-type with the maximum output coefficient TEG.<sup>169</sup> Maximum PF of n-type ( $1500 \mu\text{W m}^{-1} \text{K}^{-2}$  at room temperature) polyethyleneimine (PEI)-doped reported layered carbon nanotubes (SWCNT). Both p-type and n-type SWCNTs are flexible TEGs with three pairs of thermocouples and an open circuit voltage of 11.3 mV at a 27.5 K temperature gradient. The maximum output power it can generate is  $2.51 \mu\text{W}$ .<sup>170</sup> In addition, the optical switching of the poly(3-hexylthiophene) (P3HT)/CNT composite materials from p-type to n-type simplifies the production of the TE generator by having only one solution.<sup>171</sup> This is the main difference in the flexible TEG manufacturing method, as shown in ref. 170.

Choongho *et al.*<sup>99</sup> started with an emerging aqueous CNT/PVAC composite solution. At RT, the  $\sigma$  and  $k$  are  $48 \text{ S cm}^{-1}$  and  $0.34 \text{ W m}^{-1} \text{K}^{-1}$ , respectively, and the  $ZT$  is more significant than 0.006, containing 20 wt% CNT. Furthermore, they achieved encouraging  $ZT$  values around 0.02, and PEDOT:PSS doped with DMSO employed a network of the conductive polymer.<sup>53</sup> SWCNT added 35 wt% to PEDOT:PSS, which resulted in the  $\sigma$  reaching  $400 \text{ S cm}^{-1}$ . Yao *et al.*<sup>172</sup> found that the SWCNT/PANi nanocomposites exhibit outstanding  $S$  compared to pristine PANi. This can be attributed to improved carrier mobility in the structured chain of PANi. In contrast to pure polyaniline, composites have a maximum  $\sigma$  of  $1.25 \times 10^4 \text{ S cm}^{-1}$ , a maximum  $S$  of  $40 \mu\text{V K}^{-1}$ , and the highest PF of  $2 \times 10^4 \mu\text{W m}^{-1} \text{K}^{-2}$ . In this study, Wang *et al.*<sup>173</sup> prepared nanocomposites via a mechanical ball mill, followed by cold pressing when graphite content was present in materials at a 50 wt% concentration. The  $\sigma$  and  $S$  increase as the graphite content increases, yielding a PF of  $418 \mu\text{W m}^{-1} \text{K}^{-2}$  and  $ZT$  of  $1.37 \times 10^3$ . Yu *et al.*<sup>63</sup> described the development of a separate CNT network in a composite made of polyvinyl acetate (PVAc). A minimal amount of CNT content is crucial for creating this polymer composite because it helps to develop its distinctive properties. The creation of the CNT network enhances electrical conductivity, but the  $k$  and  $S$  parameters are unaffected by the filler concentration. The insulating polyvinyl acetate matrix uses a long drying method at ambient temperature to create a 3-D network. A thermally isolated but electrically connected network assists in improving the figure of merit. PVAc/CNTs exhibit  $\sigma$  and  $k$  values of  $48 \text{ S cm}^{-1}$  and  $0.34 \text{ W m}^{-1} \text{K}^{-1}$ , respectively, twenty wt% content of CNT at 300 K. The CNT/polymer composite can maintain conductivity that remains constant when electrical conductivity is greatly improved by the connecting junction between the CNTs.<sup>174</sup> Contrary to PVAc/CNT-filled composites, PANI-based carbon nanotube-filled composites have a decoupling effect connected to an enhanced  $S$ . SWCNT uses *in situ* polymerisation processes to create composites. Compared to polyaniline and pristine CNT, their  $S$  is  $2.74 \mu\text{V K}^{-1}$  and  $12.2 \mu\text{V K}^{-1}$ ,<sup>175</sup> whereas the PANi/CNT composite exhibits improvement performance with the highest value of up to  $28 \mu\text{V K}^{-1}$  and behaves as a p-type thermoelectric material at 350 K. The primary explanation for this is the energy-altering phenomenon that emerged with CNT and PANi contact. Kinge *et al.*<sup>176</sup> designed a labelled chemical process to





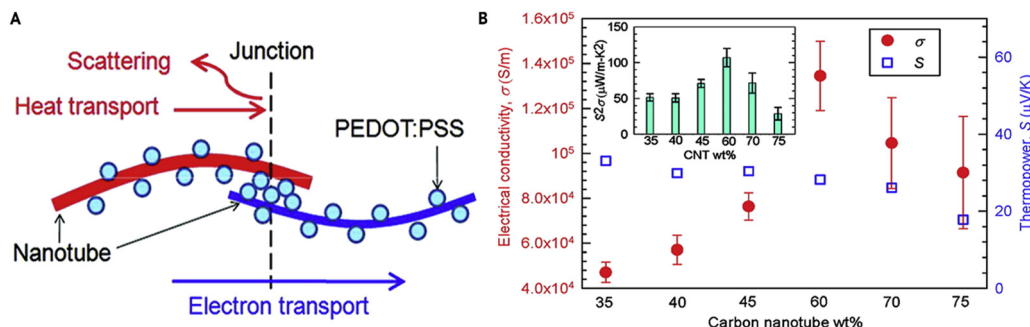


**Fig. 8** (A) Graphical representation of the interconnection of CNTs covered by PEDOT:PSS materials. (B) Electrical conductivities and Seebeck coefficients of the composites at various nanotube concentrations, with an inset illustrative of the TE power factor. Adapted with permission from ref. 63. Copyright 2011, American Chemical Society.

create CNT/polyaniline nanocomposites. The straightforward procedure starts with mixing solid ammonium peroxydisulfate with anilinium hydrochloride and CNT. By maintaining a constant CNT concentration and changing the type of CNT, the author of this work highlighted the properties of polymer nanocomposites, such as their SWCNT, MWCNT, oxidised, or unoxidised states. In comparison to the pure PANi sample, all nanohybrids exhibited superior performance. They showed excellent thermoelectric properties of PANi/unoxidised SWCNT reporting ( $\sigma$  530 S cm<sup>-1</sup>,  $S$  33  $\mu\text{V K}^{-1}$ , and PF 0.6  $\mu\text{W m}^{-1} \text{K}^{-2}$ ) in contrast to other hybrids. This nanohybrid, encompassing oxidised and unoxidised SWCNT or MWCNT, showed the same  $S$  with different  $\sigma$ . Similarly, Yu *et al.*<sup>63</sup> demonstrated a schematic PEDOT:PSS-coated carbon nanotube junction, as depicted in Fig. 8(A). A graphic depiction of the fluctuation of  $\sigma$  and  $S$  with CNT concentrations can be found in Fig. 8(B).  $\sigma$  increases with CNT concentration until a point of 60 wt%. At this point, it starts to decrease. With the change in CNT concentration,  $S$  exhibited slight changes. With the inclusion of CNT, TE characteristics have been attained. At room temperature, this alteration resulted in a maximum  $ZT$  of  $7.2 \times 10^{-5}$ .

Hewitt *et al.*<sup>142</sup> processed TE fabrics made of several CNT/polymer composite layers. CNT/polymer composite thin films have a low  $ZT$  (0.02). The author created MWCNT-filled polyvinylidene fluoride (PVDF) composite films for this assignment.

These films were stacked to produce numerous element modules that resembled felt fabric. Each layer works together to provide a greater thermoelectric voltage, which makes it a desirable alternative to materials based on bismuth telluride for TE applications.<sup>177</sup> The  $k$ ,  $\sigma$ , and PF of the GO/CNT (1:2 ratio) film improved significantly, obtaining results of 28.6 W m<sup>-1</sup> K<sup>-1</sup>,  $6.52 \times 10$  S cm<sup>-1</sup>, and  $5.33 \times 10^{-2}$   $\mu\text{W m}^{-1} \text{K}^{-2}$ , respectively. A flexible two-pair TEG was produced using SWCNT/PEDOT:PSS or TiS<sub>2</sub>/C<sub>60</sub> hybrid film as the n-type or p-type, respectively, at 20 K with 335 nW of electrical output.<sup>178</sup> Furthermore, screen printing was used to create rolled flexible TE generators by employing the p-type and n-type materials PEDOT:PSS and CPE/CNT nanocomposites, respectively.<sup>179</sup> The highest power output and open-circuit voltage of the 288-leg thermoelectric module are 46  $\mu\text{W}$  and 260 mV at 65 K, respectively. Similarly, Du *et al.*<sup>145</sup> synthesised an MWCNT/P<sub>3</sub>HT composite *via* oxidative polymerisation of 3-hexylthiophene in an MWCNT-dispersed chloroform solution. When the temperature increases from 298 to 423 K, the  $\sigma$  decreases from 0.13 to 0.11 S cm<sup>-1</sup>, and the  $S$  increases from 9.7 to 11.3  $\mu\text{V K}^{-1}$ . After cold pressing, the MWCNT content was 30 wt% in composite powder.

The structural characteristics of these composites play a significant role in determining their mechanical, thermal, electrical, and other properties. For the first time, Soltani<sup>180</sup> reported the effective use of traditional and substrate vibration-assisted ultrasonic spray coating (SVASC) to fabricate highly conductive transparent graphene-doped PEDOT:PSS composite thin films. The mechanism of dispersion of graphene in PEDOT:PSS aqueous solution using IPA is elucidated. The -OH groups in IPA can form a connection with the unsaturated carbons at the outermost edges of the broken graphene sheets. These -OH groups combine with sulphur on the hydrophilic sides of PEDOT:PSS or PSS to generate hydrogen bonds after being mixed with an aqueous solution of PEDOT:PSS. These intermolecular interactions help graphene disperse and suspend in the solution, which improves the conductivity of graphene-doped PEDOT:PSS. Fig. 9 displays the FTIR peaks of the pure PEDOT:PSS, IPA/graphene, and IPA/graphene/PEDOT:PSS solutions to support the previously mentioned assertion. The graphene surface interacts with the -OH group in IPA or water to create C-O...H bonds, which are shown by the

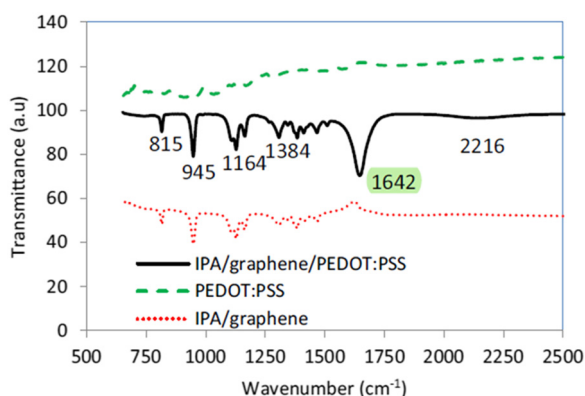


**Fig. 9** FTIR spectra of pristine PEDOT:PSS, IPA/graphene/PEDOT:PSS and IPA/graphene solution.<sup>180</sup>

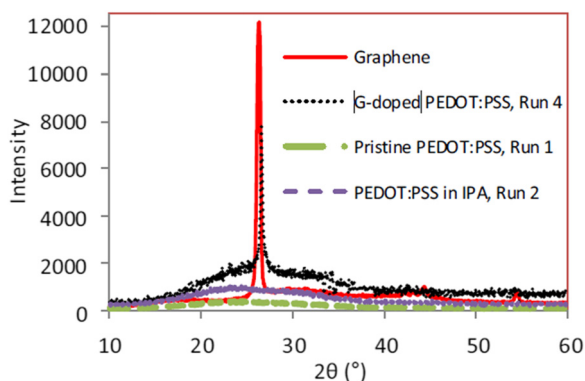


Fig. 10 XRD patterns of graphene, pristine PEDOT:PSS thin film (run 1), PEDOT:PSS thin film prepared using IPA as a co-solvent (run 2), and SVAC-fabricated graphene-doped PEDOT:PSS (run 4).<sup>180</sup>

spikes at 1301, 1164, and 1384  $\text{cm}^{-1}$ . In IPA and PEDOT:PSS solution, these interactions oversee the full and stable dispersion of graphene.<sup>181</sup> Fig. 10 displays the XRD patterns of pure graphene and graphene-doped PEDOT:PSS composite films that were IPA treated. All the PEDOT:PSS films typically exhibit a low-intensity peak of pristine PEDOT:PSS at  $23^\circ$  in their pattern.<sup>182,183</sup> The peaks of pure PEDOT:PSS and IPA/PEDOT:PSS are nearly overlapped. A prominent peak at  $26^\circ$  overlaid on the PEDOT:PSS pattern for the graphene-PEDOT:PSS thin film clearly shows the graphene's dispersion throughout the PEDOT:PSS matrix and makes evident the graphene's noteworthy influence on the conductivity of the PEDOT:PSS film. The investigation yielded a maximum electrical conductivity of  $298 \text{ S cm}^{-1}$  for a thin film composed of graphene-doped PEDOT:PSS. This value represents a ten-fold enhancement when compared to the electrical conductivity of pristine PEDOT:PSS thin films. Similarly, Du<sup>184</sup> reported that PEDOT:PSS/GQD composites were effectively made using simple casting techniques. PEDOT and PSS chains are decoupled and separated into phases because of the strong interactions between GQD and PEDOT chains *via*  $\pi$ - $\pi$  bonding. The microstructures (P-GQDs-10 wt%) that were developed simultaneously improved the electrical conductivity and Seebeck coefficient of PEDOT:PSS. When compared to pristine PEDOT:PSS, the PF of PEDOT:PSS/GQDs was increased by 550%. This work offered a viable path for the application of PEDOT:PSS in highly effective TE conversion. Analysis using Raman spectroscopy and X-ray photoelectron spectroscopy (XPS) revealed the strong  $\pi$ - $\pi$  interaction that promoted the dispersion of graphene and PEDOT:PSS. The  $ZT$  value and PF of the composite thin film with 2 wt% graphene were 0.02 and  $11.09 \mu\text{W m}^{-1} \text{ K}^{-2}$ , respectively. This improvement results from both graphene's high electron mobility ( $200\,000 \text{ cm}^2 \text{ V}^{-1} \text{ s}^{-1}$ ) and the easier carrier transfer between PEDOT:PSS and graphene.<sup>130</sup>

### 3. Graphene-based TE applications

Owing to significant advancements in the thermoelectric properties of graphene and the creation of numerous graphene-based TE

composites, scientists have already implemented these graphene-based thermoelectric materials into their devices. Moreover, graphene has demonstrated success in enhancing thermoelectric properties,<sup>94–98,185</sup> and various fascinating uses outside of cooling and power harvesting, several of which have high market value.

#### 3.1 Generator

A flexible graphene-based thermoelectric generator with seven units and a wristband design is developed by building rGO film over a controlled porosity 3D-printed poly(dimethyl siloxane) (PDMS) grid (Fig. 11a and b). This allows for a lightweight, thinner, and more foldable device. At a  $\Delta T$  of 50 K, it gives an output of  $57.33 \text{ mV g}^{-1}$  at an atmospheric<sup>94</sup> temperature of 288 K, achieving a maximum power density of  $4.19 \mu\text{W g}^{-1}$ . Because of Young's modulus and the great flexibility of PDMS, the TE generator can be used in self-powered wearable micro-electronic devices.

#### 3.2 Supercapacitors

Owing to their mechanical rigidity, conventional inorganic supercapacitors cannot be heated to charge them and, therefore, cannot be used in wearable applications. A novel planar supercapacitor that can be thermally set was created by Kim *et al.*<sup>95</sup> based on the thermoelectric feature of graphene, as shown in Fig. 11c. Liquid-phase electrolytes were not used to generate the supercapacitor. Here, the transport effect drives the Soret mechanism, permitting the generation of  $S$  up to  $9 \mu\text{V K}^{-1}$ . The ultrahigh  $S$  with superb  $\sigma$  results from the boosted charge mobility and concentration of protons on the SGO electrode, and the regenerated electricity is stored simultaneously. The single device produces a significant thermally generated charge voltage of 58 mV at a temperature of 10.5 K. The gadgets can even create a power of up to 2.1 V. When arranged in an array (Fig. 11d), they are suited for large-scale production.

#### 3.3 Cell

Yang *et al.*<sup>96</sup> created a thermoelectric cell based on nanoporous graphene, as shown in Fig. 11e. Two graphene electrodes connect both ends: the hot and cold ends of the closed TE cell. The cell was allowed to capture energy because of the rearrangement of the double electric layer between the electrodes at a specific temperature. The voltage generated at 35 K was 168.91 mV, corresponding to an  $S$  of  $4.54 \mu\text{V K}^{-1}$ , which is much greater than that of conventional thermoelectric generators. The large and wide specific surfaces of the nanoporous graphene-based electrodes facilitated this.

#### 3.4 Sensor

Graphene is suitable for self-powered wearable sensors because of its TE characteristics, flexibility, and affordability. Based on the TE characteristics of elastics, flexible, freestanding, and thin rGO foam, Hou *et al.*<sup>97</sup> described facile and self-powered thin-film sensors with superior flexibility. High conductivity sensors have been reported to differentiate human touch from



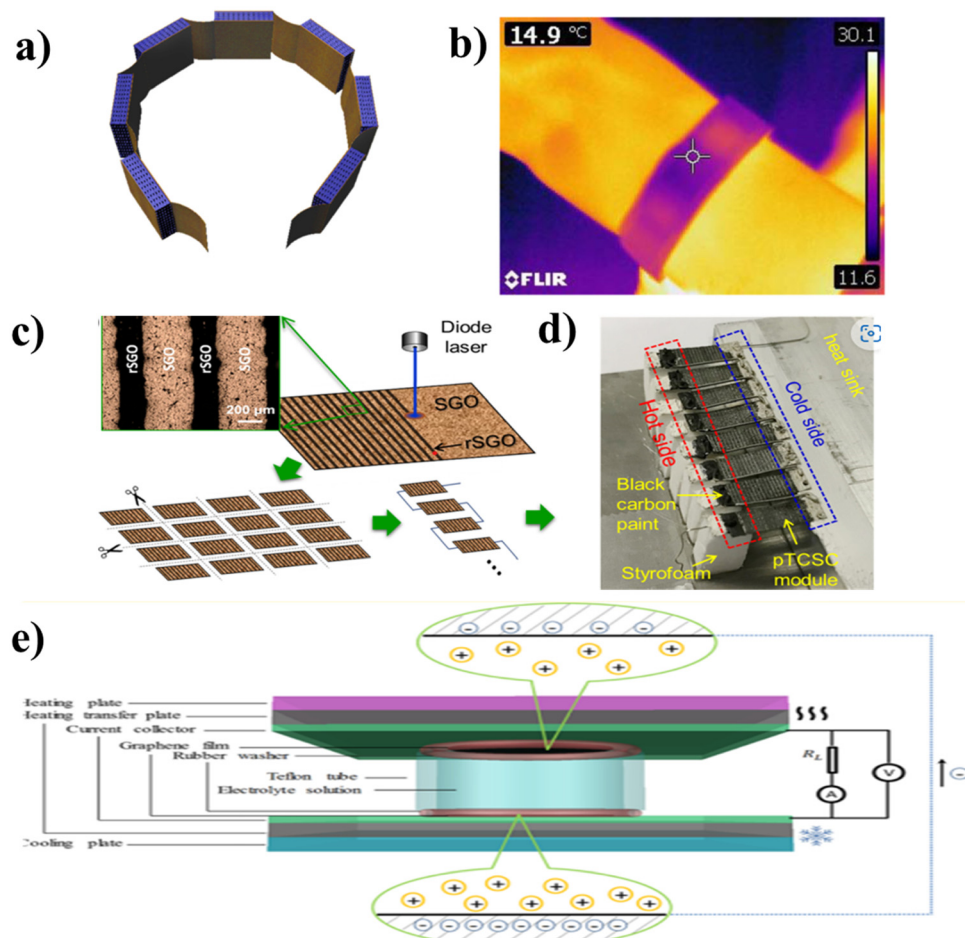


**Fig. 11** (a) Design of the graphene-based thermoelectric generator. (b) Spectrum of a wristband-style generator of thermal infrared radiation, with permission from Elsevier. Panels a and b are republished from ref. 94, copyright 2018. (c) SGO/rSGO patterns are created through laser-assisted SGO reduction, minor module tailoring, and series connections. (d) A generator is made up of interconnected modules. Panels c and d are reproduced from ref. 95, copyright 2018, with permission from Elsevier. (e) Graphene-based closed TE cell schematic, adapted from ref. 96 with permission from ACS, copyright 2019.

other pressures, which can measure weight, pressure behaviour, and pressure levels. This might be helpful for future robot generations. Zhang *et al.*<sup>98</sup> created a graphene/eco-flex hybrid film-based, self-powered, and ultrasensitive system to strain the system. It uses excellent tensile properties in the eco-flex elastomer and good TE performance in graphene. The sensor displays good strain resolution and outstanding stability under repeated strains. Based on the  $\Delta T$  between the skin and the surroundings, it can detect small movements with great precision when in contact with human skin.

## 4. Conclusions, challenges and future scope

Wearable technology and other TE-based functional materials promote graphene-based thermoelectrics as a viable alternative. Nowadays, research in the science and engineering of graphene has continued and provides strong technical and theoretical evidence for its continued support for its continued

thermoelectric performance optimisation, which is still necessary for practical applications in various fields. Additionally, the efficient and improved large-scale manufacture of graphene has established a solid foundation for the exciting future of graphene-based thermoelectric devices. Efficient thermoelectric materials are necessary for converting waste heat into usable electrical energy in thermoelectric power generators. The most promising 2D nanomaterials are those with high Seebeck coefficients and low thermal conductivity. These materials should also be able to transfer electrical energy into thermal energy without any damage or loss of energy. Thermoelectric properties are influenced by the doping level, carrier concentration, and mobility of graphene. The Seebeck coefficient of undoped graphene is  $76 \mu\text{V K}^{-1}$ , while the PAA-doped and PEI-doped graphene have Seebeck coefficients of 115 and  $70 \mu\text{V K}^{-1}$ , respectively.

In addition to improving the Seebeck coefficient, increasing the carrier concentration and mobility of graphene can reduce its thermal conductivity by reducing its lattice contribution. This can improve the performance of graphene-based



thermoelectric devices and make them more economical for thermoelectric power generation. Moreover, the thermal conductivity of graphene can be improved using chemical doping methods to enhance the electron concentration and mobility of the active layer of graphene. In this study, graphene was used to demonstrate the performance of the composites. The results show that doping can enhance the carrier concentration and mobility of the active layer by at least 200%. This improved the thermoelectric power conversion efficiency and the power factor by at least 600%.

In recent years, researchers have been able to produce large-area monolayer graphene devices with thermoelectric properties comparable to or better than those of single-layer graphene devices. However, graphene-based devices require a significant effort to fabricate them because of the difficulty in producing large-area monolayer graphene and sintering them into a homogeneous structure as well as the need for obtaining thermoelectric properties with a uniform energy transfer across the graphene sheets. One of the most exciting properties of graphene is its  $sp^2$  hybridisation of carbon atoms, which leads to a hexagonal honeycomb structure that is only one atom thick. In addition, graphene possesses non-covalent solid interactions between the carbon atoms, which offer stability to the graphene and improve its thermal, electrical, and mechanical properties. In addition, graphene can withstand extremely high currents and quickly balance out missing charges, making it an attractive candidate for future electronic applications. Another potential application of graphene is in organic composites. Graphene can be incorporated into organic polymers to improve their physical and chemical properties. Graphene can improve the permeability of a polymer and increase its tensile strength and toughness. In addition, graphene can be incorporated into a polymer to increase its thermal conductivity and in-plane electrical resistivity. Graphene can also be incorporated into organic coatings, such as polyurethanes, to enhance their performance in electrochemical and thermal transport processes.

It is necessary to improve the carrier concentration and mobility to improve the thermal conductivity and in-plane electrical resistance of graphene. Hence, inorganic graphene-based composites are expected to significantly increase the TE performance of graphene. TE devices based on graphene + inorganic composites have the potential to achieve a high  $ZT$  of up to 2. To improve the long-term cycling performance of graphene, it is necessary to decrease the temperature gradient between electrodes. To do this, we fabricated a graphene + inorganic composite using a polymer blend of phosphorus-doped graphene and magnesium. To determine the thermal conductivity of this composite, a Peltier device was fabricated with a temperature difference in the range of 323–353 K between the graphene electrodes. Then, the resulting thermoelectric voltage was measured using a commercial graphene voltage meter.

Graphene-based materials are becoming increasingly popular in the TE industry owing to their superior electrical transport, thermal stability, and mechanical properties. Graphene



Fig. 12 Key challenges in developing OTE materials.

and its derivatives have exhibited tunable TE properties and have been proven effective in enhancing TE performance when operating as an infill in polymers or as a second phase in inorganic TE composites. In addition, graphene-based TEs are a competitive option for wearable devices and other TE-based functional materials. Today, scientific and engineering studies on the physics and chemistry of graphene have provided strong theoretical and technological support for the further optimization of graphene-based TE performance, which is still required for practical applications. Furthermore, the large-scale production of graphene has reached maturity and reliability, laying a solid foundation for the future of graphene-based TEs.

Developing organic thermoelectric (OTE) materials is challenging because of their unique properties and requirements for thermoelectric applications.<sup>35</sup> The following are some of the key challenges [Fig. 12]. Owing to their low electrical and thermal conductivities, organic materials have difficulty achieving high thermoelectric efficiency.<sup>36,37</sup> To obtain a high thermoelectric figure of merit, it is necessary to balance these two properties simultaneously.<sup>186</sup> Several factors can make an organic material sensitive to the environment, including moisture, oxygen, and temperature.<sup>187</sup> In particular, in harsh environments, OTE materials must maintain stability and durability over time.<sup>188</sup> Organic materials typically convert heat into electricity only over a small range of temperatures. It is crucial to expand the temperature range of OTE materials for use in various applications.<sup>189</sup> The controlled morphology and structure of OTE materials are challenging to fabricate and process.<sup>190</sup> Maximizing thermoelectric performance requires uniform films or bulk materials with optimized properties. Many organic materials are used in thermoelectric applications and are often expensive to produce or process.<sup>191</sup> Making OTE materials economically viable for widespread application





requires the development of cost-effective synthesis and fabrication methods.<sup>192</sup> Integrating organic thermoelectric materials with other components, such as electrodes and heat exchangers, can be challenging.<sup>193</sup> Ensuring compatibility and optimizing the interface between materials are crucial for overall system performance.<sup>194</sup>

Scaling up the production of OTE materials from the lab-scale to the commercial scale can be difficult.<sup>195</sup> Developing scalable manufacturing processes while maintaining desired material properties is essential for the practical implementation of OTE devices.<sup>196</sup> The pool of suitable organic materials for thermoelectric applications is relatively limited compared to inorganic materials. Expanding the range of available materials with desirable thermoelectric properties is an ongoing challenge. Achieving reliable and reproducible results in synthesizing and characterizing OTE materials is crucial for both research and commercial applications. Variability in material properties can hinder the widespread adoption of these materials.<sup>197</sup>

In organic materials, heat and charge transport are complex processes that require a deep understanding of the mechanisms involved.<sup>198</sup> Developing accurate models and theories for predicting and optimizing thermoelectric performance is ongoing.<sup>199</sup> Combining expertise from materials science, chemistry, physics, and engineering is essential to address these challenges.<sup>197</sup> Researchers and developers are currently working on overcoming these obstacles to harness the full potential of organic thermoelectric materials for energy harvesting and conversion.<sup>200</sup>

The future trajectory of practical TE applications necessitates the identification and resolution of pivotal challenges, as well as the exploration of novel solutions aimed at augmenting efficiency, cost effectiveness, and versatility. Here are few possible directions for TE devices in real-world applications. The advancement of research in graphene-based TE materials has resulted in accelerated progress in the integration of these materials into TE devices. This integration extends beyond flexible TE electronics and encompasses applications in energy harvesting, wearable electronic automotive industry, aerospace applications, medical devices efficient heat exchange, Internet of Things (IoT), climate control and refrigeration, flexible and portable electronics, machine learning and optimization and other areas. The incorporation of graphene into various functional devices has significantly expanded the potential applications of graphene and its derivatives, particularly in relation to its TE properties. Although still in the early stages of development, these advancements have the potential to greatly impact various markets. By concentrating on these areas, scientists and engineers may help bring TE technology closer to real-world applications in various fields, such as energy harvesting and wearable electronics. This comprehensive strategy will be crucial in determining how TE applications will develop in the future.

## Conflicts of interest

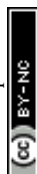
There are no conflicts to declare.

## Acknowledgements

Vaishali Rathi would like to express gratitude to UPES, Dehradun for providing research fellowship. Ashish Kumar would like to acknowledge the funding received from SERB, India through SRS scheme.

## References

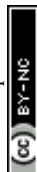
- 1 Y. Lee, D.-Y. Jo, T. Kim, J.-H. Jo, J. Park, H. Yang and D. Kim, Interfaces, Effectual interface and defect engineering for auger recombination suppression in bright InP/ZnSeS/ZnS quantum dots, *ACS Appl. Mater. Interfaces*, 2022, **14**(10), 12479–12487.
- 2 L. Zhang, B. Xia, X.-L. Shi, W.-D. Liu, Y. Yang, X. Hou, X. Ye, G. Suo and Z.-G. Chen, Achieving high thermoelectric properties in PEDOT:PSS/SWCNTs composite films by a combination of dimethyl sulfoxide doping and NaBH<sub>4</sub> dedoping, *Carbon*, 2022, **196**, 718–726.
- 3 E. Motoasca, Environments, Energy sustainability through the use of thermoelectric materials in waste heat recovery systems recent developments and challenges, *Energy Sustainability Built Urban Environ.*, 2019, 237–254.
- 4 H. Wang and C. Yu, Organic Thermoelectrics: Materials Preparation, Performance Optimization, and Device Integration, *Joule*, 2019, **3**(1), 53–80.
- 5 G. J. Snyder and E. S. Toberer, Complex thermoelectric materials, *Nat. Mater.*, 2008, **7**(2), 105–114.
- 6 S. Lal, D. Gautam and K. M. Razeed, Fabrication of micro-thermoelectric devices for power generation and the thermal management of photonic devices, *J. Micromech. Microeng.*, 2019, **29**(6), 065015.
- 7 R. D. I. G. Dharmasena, K. D. G. I. Jayawardena, Z. Saadi, X. Yao, R. M. I. Bandara, Y. Zhao and S. R. P. Silva, Energy Scavenging and Powering E-Skin Functional Devices, *Proc. IEEE*, 2019, **107**(10), 2118–2136.
- 8 M. H. Malakooti, N. Kazem, J. Yan, C. Pan, E. J. Markvicka, K. Matyjaszewski and C. Majidi, Liquid Metal Supercooling for Low-Temperature Thermoelectric Wearables, *Adv. Funct. Mater.*, 2019, **29**(45), 1906098.
- 9 S.-J. Chen and Y.-C. Wu, Active Thermoelectric Vacuum Sensor Based on Frequency Modulation, *Micromachines*, 2020, **11**(1), 15.
- 10 D. Newell and M. Duffy, Review of Power Conversion and Energy Management for Low-Power, Low-Voltage Energy Harvesting Powered Wireless Sensors, *IEEE Trans. Power Electron.*, 2019, **34**(10), 9794–9805.
- 11 T. J. Seebeck, *Ueber den Magnetismus der galvanischen Kette*, 1822.
- 12 J. C. A. Peltier, *Nouvelles expériences sur la calorité des courants électriques*, 1834.
- 13 W. Thomson, 4. On a Mechanical Theory of Thermoelectric Currents, *Proc. R. Soc. Edinburgh*, 1857, **3**, 91–98.
- 14 M. S. Dresselhaus, G. Chen, M. Y. Tang, R. G. Yang, H. Lee, D. Z. Wang, Z. F. Ren, J.-P. Fleurial and P. Gogna, New



- Directions for Low-Dimensional Thermoelectric Materials, *Adv. Mater.*, 2007, **19**(8), 1043–1053.
- 15 L. Pan, X. L. Shi, C. Song, W. D. Liu, Q. Sun, C. Lu, Q. Liu, Y. Wang and Z. G. Chen, Graphite Nanosheets as Multi-functional Nano-inclusions to Boost the Thermoelectric Performance of the Shear-Exfoliated Bi<sub>2</sub>O<sub>2</sub>Se, *Adv. Funct. Mater.*, 2022, **32**(30), 2202927.
  - 16 Q.-X. Hu, W.-D. Liu, L. Zhang, W. Sun, H. Gao, X.-L. Shi, Y.-L. Yang, Q. Liu and Z.-G. Chen, SWCNTs/Ag<sub>2</sub>Se film with superior bending resistance and enhanced thermoelectric performance via *in situ* compositing, *Chem. Eng. J.*, 2023, **457**, 141024.
  - 17 X.-Y. Mao, X.-L. Shi, L.-C. Zhai, W.-D. Liu, Y.-X. Chen, H. Gao, M. Li, D.-Z. Wang, H. Wu and Z.-H. Zheng, High thermoelectric and mechanical performance in the n-type polycrystalline SnSe incorporated with multi-walled carbon nanotubes, *J. Mater. Sci. Technol.*, 2022, **114**, 55–61.
  - 18 L. Deng, Y. Liu, Y. Zhang, S. Wang and P. Gao, Organic Thermoelectric Materials: Niche Harvester of Thermal Energy, *Adv. Funct. Mater.*, 2023, **33**(3), 2210770.
  - 19 Y. Liu, J. Zhi, W. Li, Q. Yang, L. Zhang and Y. Zhang, Oxide materials for thermoelectric conversion, *Molecules*, 2023, **28**(15), 5894.
  - 20 F. Ali and M. Koc, 3D Printed Polymer Piezoelectric Materials: Transforming Healthcare through Biomedical Applications, *Polymers*, 2023, **15**(23), 4470.
  - 21 X. Li, C. Wan, T. Tao, H. Chai, Q. Huang, Y. Chai and Y. Wu, An overview of the development status and applications of cellulose-based functional materials, *Cellulose*, 2023, 1–39.
  - 22 A. K. Katiyar, A. T. Hoang, D. Xu, J. Hong, B. J. Kim, S. Ji and J.-H. Ahn, 2D Materials in Flexible Electronics: Recent Advances and Future Prospectives, *Chem. Rev.*, 2023, DOI: [10.1021/acs.chemrev.3c00302](https://doi.org/10.1021/acs.chemrev.3c00302).
  - 23 A. M. Al-Amri, Recent Progress in Printed Photonic Devices: A Brief Review of Materials, Devices, and Applications, *Polymers*, 2023, **15**(15), 3234.
  - 24 K. Jaroszevska, B. Szczęśniak, B. Szyja, J. Choma and M. Jaroniec, Inorganic mesoporous oxides: From research to industrial applications, *Mater. Today*, 2023, **67**, 23–32.
  - 25 B. G. Krishna, D. S. Ghosh and S. Tiwari, Hole and electron transport materials: A review on recent progress in organic charge transport materials for efficient, stable, and scalable perovskite solar cells, *Chem. Org. Mater.*, 2023, 100026.
  - 26 T. Tracy, L. Wu, X. Liu, S. Cheng and X. Li, 3D printing: Innovative solutions for patients and pharmaceutical industry, *Int. J. Pharm.*, 2023, **631**, 122480.
  - 27 K. Balasubramanian, A. K. Pandey, R. Abolhassani, H.-G. Rubahn, S. Rahman and Y. K. Mishra, Tetrapods based engineering of organic phase change material for thermal energy storage, *Chem. Eng. J.*, 2023, **462**, 141984.
  - 28 Z.-H. Zheng, X.-L. Shi, D.-W. Ao, W.-D. Liu, M. Li, L.-Z. Kou, Y.-X. Chen, F. Li, M. Wei and G.-X. Liang, Harvesting waste heat with flexible Bi<sub>2</sub>Te<sub>3</sub> thermoelectric thin film, *Nat. Sustain.*, 2023, **6**(2), 180–191.
  - 29 S. Lan, Q. Li, X. Guo, S. Wang and R. Chen, Fuel saving potential analysis of bifunctional vehicular waste heat recovery system using thermoelectric generator and organic Rankine cycle, *Energy*, 2023, **263**, 125717.
  - 30 M. Asaduzzaman, M. H. Ali, N. A. Pratik and N. Lubaba, Exhaust Heat Harvesting of Automotive Engine Using Thermoelectric Generation Technology, *Energy Convers. Manage.*, 2023, 100398.
  - 31 J. Caban, J. Vrabel, D. Górnicka, R. Nowak, M. Jankiewicz, J. Matijošius and M. Palka, Overview of Energy Harvesting Technologies Used in Road Vehicles, *Energies*, 2023, **16**(9), 3787.
  - 32 P. Judeinstein and C. Sanchez, Hybrid organic–inorganic materials: a land of multidisciplinary, *J. Mater. Chem.*, 1996, **6**(4), 511–525.
  - 33 X.-L. Shi, J. Zou and Z.-G. Chen, Advanced thermoelectric design: from materials and structures to devices, *Chem. Rev.*, 2020, **120**(15), 7399–7515.
  - 34 Y. Sun, C. A. Di, W. Xu and D. Zhu, Advances in n-type organic thermoelectric materials and devices, *Adv. Electron. Mater.*, 2019, **5**(11), 1800825.
  - 35 Y. H. Pai, J. Tang, Y. Zhao and Z. Liang, Ionic Organic Thermoelectrics with Impressively High Thermopower for Sensitive Heat Harvesting Scenarios, *Adv. Energy Mater.*, 2023, **13**(1), 2202507.
  - 36 B. N. Stram, Key challenges to expanding renewable energy, *Energy Policy*, 2016, **96**, 728–734.
  - 37 Q. Zhang, Y. Sun, W. Xu and D. Zhu, Organic thermoelectric materials: emerging green energy materials converting heat to electricity directly and efficiently, *Adv. Mater.*, 2014, **26**(40), 6829–6851.
  - 38 M. Vedernikov and E. Iordanishvili, AF Ioffe and origin of modern semiconductor thermoelectric energy conversion, Seventeenth International Conference on Thermoelectrics. Proceedings ICT98 (Cat. No. 98TH8365), IEEE, 1998, pp. 37–42.
  - 39 C. Goupil, W. Seifert, K. Zabrocki, E. Müller and G. Snyder, Thermodynamics of Thermoelectric Phenomena and Applications, *Entropy*, 2011, **13**, 1481–1517.
  - 40 J. P. Heremans, V. Jovic, E. S. Toberer, A. Saramat, K. Kurosaki, A. Charoenphakdee, S. Yamanaka and G. J. Snyder, Enhancement of thermoelectric efficiency in PbTe by distortion of the electronic density of states, *Science*, 2008, **321**(5888), 554–557.
  - 41 H. Ohta, S. Kim, Y. Mune, T. Mizoguchi, K. Nomura, S. Ohta, T. Nomura, Y. Nakanishi, Y. Ikumura, M. Hirano, H. Hosono and K. Koumoto, Giant thermoelectric Seebeck coefficient of a two-dimensional electron gas in SrTiO<sub>3</sub>, *Nat. Mater.*, 2007, **6**(2), 129–134.
  - 42 P. Reddy, S.-Y. Jang, R. A. Segalman and A. Majumdar, Thermoelectricity in Molecular Junctions, *Science*, 2007, **315**(5818), 1568–1571.
  - 43 J. N. Coleman, M. Lotya, A. O'Neill, S. D. Bergin, P. J. King, U. Khan, K. Young, A. Gaucher, S. De, R. J. Smith, I. V. Shvets, S. K. Arora, G. Stanton, H.-Y. Kim, K. Lee, G. T. Kim, G. S. Duesberg, T. Hallam, J. J. Boland, J. J. Wang, J. F. Donegan, J. C. Grunlan, G. Moriarty, A. Shmeliov, R. J. Nicholls, J. M. Perkins, E. M. Grievson, K. Theuwissen,



- D. W. McComb, P. D. Nellist and V. Nicolosi, Two-Dimensional Nanosheets Produced by Liquid Exfoliation of Layered Materials, *Science*, 2011, **331**(6017), 568–571.
- 44 L. Shi, D. Li, C. Yu, W. Jang, D. Kim, Z. Yao, P. Kim and A. Majumdar, Measuring Thermal and Thermoelectric Properties of One-Dimensional Nanostructures Using a Microfabricated Device, *J. Heat Transfer*, 2003, **125**(5), 881–888.
- 45 D. Vashaee and A. Shakouri, Improved Thermoelectric Power Factor in Metal-Based Superlattices, *Phys. Rev. Lett.*, 2004, **92**(10), 106103.
- 46 A. I. Boukai, Y. Bunimovich, J. Tahir-Kheli, J.-K. Yu, W. A. Goddard III and J. R. Heath, Silicon nanowires as efficient thermoelectric materials, *Nature*, 2008, **451**(7175), 168–171.
- 47 J. Tang, H.-T. Wang, D. H. Lee, M. Fardy, Z. Huo, T. P. Russell and P. Yang, Holey Silicon as an Efficient Thermoelectric Material, *Nano Lett.*, 2010, **10**(10), 4279–4283.
- 48 Q. Zhang, Y. Sun, W. Xu and D. Zhu, What To Expect from Conducting Polymers on the Playground of Thermoelectricity: Lessons Learned from Four High-Mobility Polymeric Semiconductors, *Macromolecules*, 2014, **47**(2), 609–615.
- 49 Y. Chen, Y. Zhao and Z. Liang, Solution processed organic thermoelectrics: towards flexible thermoelectric modules, *Energy Environ. Sci.*, 2015, **8**(2), 401–422.
- 50 J. Kim and J.-H. Lim, Organic-Inorganic Hybrid Thermoelectric Material Synthesis and Properties, *J. Korean Ceram. Soc.*, 2017, **54**, 272–277.
- 51 R. Prasad and S. Bhamre, Review on texturization effects in thermoelectric oxides, *Mater. Renew. Sustain. Energy*, 2020, **9**, 3.
- 52 C. Yu, Y. S. Kim, D. Kim and J. C. Grunlan, Thermoelectric Behavior of Segregated-Network Polymer Nanocomposites, *Nano Lett.*, 2008, **8**(12), 4428–4432.
- 53 D. Kim, Y. Kim, K. Choi, J. C. Grunlan and C. Yu, Improved Thermoelectric Behavior of Nanotube-Filled Polymer Composites with Poly(3,4-ethylenedioxythiophene) Poly(styrene-sulfonate), *ACS Nano*, 2010, **4**(1), 513–523.
- 54 O. Bubnova, Z. U. Khan, A. Malti, S. Braun, M. Fahlman, M. Berggren and X. Crispin, Optimization of the thermoelectric figure of merit in the conducting polymer poly(3,4-ethylenedioxythiophene), *Nat. Mater.*, 2011, **10**(6), 429–433.
- 55 H. Wang, J.-H. Hsu, S.-I. Yi, S. L. Kim, K. Choi, G. Yang and C. Yu, Thermally Driven Large N-Type Voltage Responses from Hybrids of Carbon Nanotubes and Poly(3,4-ethylenedioxythiophene) with Tetrakis(dimethylamino)ethylene, *Adv. Mater.*, 2015, **27**(43), 6855–6861.
- 56 L.-D. Zhao, S.-H. Lo, Y. Zhang, H. Sun, G. Tan, C. Uher, C. Wolverton, V. P. Dravid and M. G. Kanatzidis, Ultralow thermal conductivity and high thermoelectric figure of merit in SnSe crystals, *Nature*, 2014, **508**(7496), 373–377.
- 57 O. Bubnova and X. Crispin, Towards polymer-based organic thermoelectric generators, *Energy Environ. Sci.*, 2012, **5**(11), 9345–9362.
- 58 M. He, F. Qiu and Z. Lin, Towards high-performance polymer-based thermoelectric materials, *Energy Environ. Sci.*, 2013, **6**(5), 1352–1361.
- 59 T. O. Poehler and H. E. Katz, Prospects for polymer-based thermoelectrics: state of the art and theoretical analysis, *Energy Environ. Sci.*, 2012, **5**(8), 8110–8115.
- 60 N. Toshima, Recent progress of organic and hybrid thermoelectric materials, *Synth. Met.*, 2017, **225**, 3–21.
- 61 C. Cho, K. L. Wallace, P. Tzeng, J.-H. Hsu, C. Yu and J. C. Grunlan, Outstanding Low Temperature Thermoelectric Power Factor from Completely Organic Thin Films Enabled by Multidimensional Conjugated Nanomaterials, *Adv. Energy Mater.*, 2016, **6**(7), 1502168.
- 62 H. Wang, S.-I. Yi, X. Pu and C. Yu, Simultaneously Improving Electrical Conductivity and Thermopower of Polyaniline Composites by Utilizing Carbon Nanotubes as High Mobility Conduits, *ACS Appl. Mater. Interfaces*, 2015, **7**(18), 9589–9597.
- 63 C. Yu, K. Choi, L. Yin and J. C. Grunlan, Light-Weight Flexible Carbon Nanotube Based Organic Composites with Large Thermoelectric Power Factors, *ACS Nano*, 2011, **5**(10), 7885–7892.
- 64 K. C. See, J. P. Feser, C. E. Chen, A. Majumdar, J. J. Urban and R. A. Segalman, Water-Processable Polymer–Nanocrystal Hybrids for Thermoelectrics, *Nano Lett.*, 2010, **10**(11), 4664–4667.
- 65 N. E. Coates, S. K. Yee, B. McCulloch, K. C. See, A. Majumdar, R. A. Segalman and J. J. Urban, Effect of Interfacial Properties on Polymer–Nanocrystal Thermoelectric Transport, *Adv. Mater.*, 2013, **25**(11), 1629–1633.
- 66 M. Cutler, J. F. Leavy and R. L. Fitzpatrick, Electronic Transport in Semimetallic Cerium Sulfide, *Phys. Rev.*, 1964, **133**(4A), A1143–A1152.
- 67 Y. Wang, J. Zhou and R. Yang, Thermoelectric Properties of Molecular Nanowires, *J. Phys. Chem. C*, 2011, **115**(49), 24418–24428.
- 68 V. Coropceanu, J. Cornil, D. A. da Silva Filho, Y. Olivier, R. Silbey and J.-L. Brédas, Charge Transport in Organic Semiconductors, *Chem. Rev.*, 2007, **107**(4), 926–952.
- 69 R. Franz and G. Wiedemann, Ueber die Wärme-Leitungsfähigkeit der Metalle, *Ann. Phys.*, 1853, **165**(8), 497–531.
- 70 C. Kittel and P. McEuen, *Introduction to solid state physics*, John Wiley & Sons, 2018.
- 71 T. Park, C. Park, B. Kim, H. Shin and E. Kim, Flexible PEDOT electrodes with large thermoelectric power factors to generate electricity by the touch of fingertips, *Energy Environ. Sci.*, 2013, **6**(3), 788–792.
- 72 M. B. Salamon, J. W. Bray, G. DePasquali, R. A. Craven, G. Stucky and A. Schultz, Thermal conductivity of tetrathiafulvalene-tetracyanoquinodimethane (TTF-TCNQ) near the metal-insulator transition, *Phys. Rev. B: Solid State*, 1975, **11**(2), 619–622.
- 73 J. Liu, X. Wang, D. Li, N. E. Coates, R. A. Segalman and D. G. Cahill, Thermal Conductivity and Elastic Constants of PEDOT:PSS with High Electrical Conductivity, *Macromolecules*, 2015, **48**(3), 585–591.



- 74 A. Weathers, Z. U. Khan, R. Brooke, D. Evans, M. T. Pettes, J. W. Andreasen, X. Crispin and L. Shi, Significant Electronic Thermal Transport in the Conducting Polymer Poly(3,4-ethylenedioxythiophene), *Adv. Mater.*, 2015, **27**(12), 2101–2106.
- 75 M. Pietralla, High thermal conductivity of polymers: Possibility or dream?, *J. Comput.-Aided Mater. Des.*, 1996, **3**(1), 273–280.
- 76 N. G. Semaltianos, C. Koidis, C. Pitsalidis, P. Karagiannidis, S. Logothetidis, W. Perrie, D. Liu, S. P. Edwardson, E. Fearon, R. J. Potter, G. Dearden and K. G. Watkins, Picosecond laser patterning of PEDOT:PSS thin films, *Synth. Met.*, 2011, **161**(5), 431–439.
- 77 R. Cagnolati, D. Fioretto, G. Ruggeri and G. Socino, Elastic characterization of poly(3-n-decylpyrrole) thin films by Brillouin light scattering, *Synth. Met.*, 1993, **60**(3), 255–258.
- 78 D. Moses and A. Denenstien, Experimental determination of the thermal conductivity of a conducting polymer: Pure and heavily doped polyacetylene, *Phys. Rev. B: Condens. Matter Mater. Phys.*, 1984, **30**(4), 2090–2097.
- 79 J. Jin, M. P. Manoharan, Q. Wang and M. A. Haque, In-plane thermal conductivity of nanoscale polyaniline thin films, *Appl. Phys. Lett.*, 2009, **95**(3), 033113.
- 80 J.-K. Wu, M. Hofmann, W.-P. Hsieh, S.-H. Chen, Z.-L. Yen, S.-K. Chiu, Y.-R. Luo, C.-C. Chiang, S.-Y. Huang, Y.-H. Chang and Y.-P. Hsieh, Enhancing Thermoelectric Properties of 2D Bi<sub>2</sub>Se<sub>3</sub> by 1D Texturing with Graphene, *ACS Appl. Energy Mater.*, 2019, **2**(12), 8411–8415.
- 81 P.-A. Zong, P. Zhang, S. Yin, Y. Huang, Y. Wang and C. Wan, Fabrication and Characterization of a Hybrid Bi<sub>2</sub>Se<sub>3</sub>/Organic Superlattice for Thermoelectric Energy Conversion, *Adv. Electron. Mater.*, 2019, **5**(11), 1800842.
- 82 K. Kanahashi, J. Pu and T. Takenobu, 2D Materials for Large-Area Flexible Thermoelectric Devices, *Adv. Energy Mater.*, 2020, **10**(11), 1902842.
- 83 C. Lee, X. Wei, J. W. Kysar and J. Hone, Measurement of the Elastic Properties and Intrinsic Strength of Monolayer Graphene, *Science*, 2008, **321**(5887), 385–388.
- 84 K. I. Bolotin, K. J. Sikes, Z. Jiang, M. Klima, G. Fudenberg, J. Hone, P. Kim and H. L. Stormer, Ultrahigh electron mobility in suspended graphene, *Solid State Commun.*, 2008, **146**(9), 351–355.
- 85 Q.-Y. Li, T. Feng, W. Okita, Y. Komori, H. Suzuki, T. Kato, T. Kaneko, T. Ikuta, X. Ruan and K. Takahashi, Enhanced Thermoelectric Performance of As-Grown Suspended Graphene Nanoribbons, *ACS Nano*, 2019, **13**(8), 9182–9189.
- 86 K. Kanahashi, M. Ishihara, M. Hasegawa, H. Ohta and T. Takenobu, Giant power factors in p- and n-type large-area graphene films on a flexible plastic substrate, *npj 2D Mater. Appl.*, 2019, **3**(1), 44.
- 87 T. Li, A. D. Pickel, Y. Yao, Y. Chen, Y. Zeng, S. D. Lacey, Y. Li, Y. Wang, J. Dai, Y. Wang, B. Yang, M. S. Fuhrer, A. Marconnet, C. Dames, D. H. Drew and L. Hu, Thermoelectric properties and performance of flexible reduced graphene oxide films up to 3,000 K, *Nat. Energy*, 2018, **3**(2), 148–156.
- 88 Z. Zhang, G. Chen, H. Wang and W. Zhai, Enhanced thermoelectric property by the construction of a nanocomposite 3D interconnected architecture consisting of graphene nanolayers sandwiched by polypyrrole nanowires, *J. Mater. Chem. C*, 2015, **3**(8), 1649–1654.
- 89 K. Zhang, S. Wang, X. Zhang, Y. Zhang, Y. Cui and J. Qiu, Thermoelectric performance of p-type nanohybrids filled polymer composites, *Nano Energy*, 2015, **13**, 327–335.
- 90 L. Wang, H. Bi, Q. Yao, D. Ren, S. Qu, F. Huang and L. Chen, Three-dimensional tubular graphene/polyaniline composites as high-performance elastic thermoelectrics, *Compos. Sci. Technol.*, 2017, **150**, 135–140.
- 91 Y. Du, K. Cai and S. Z. Shen, Facile preparation and characterization of graphene nanosheet/polyaniline nanofiber thermoelectric composites, *Funct. Mater. Lett.*, 2013, **06**(05), 1340002.
- 92 Y. Du, K. F. Cai, S. Z. Shen and P. S. Casey, Preparation and characterization of graphene nanosheets/poly(3-hexylthiophene) thermoelectric composite materials, *Synth. Met.*, 2012, **162**(23), 2102–2106.
- 93 Y. Du, S. Z. Shen, W. Yang, R. Donelson, K. Cai and P. S. Casey, Simultaneous increase in conductivity and Seebeck coefficient in a polyaniline/graphene nanosheets thermoelectric nanocomposite, *Synth. Met.*, 2012, **161**(23), 2688–2692.
- 94 W. Zeng, X.-M. Tao, S. Lin, C. Lee, D. Shi, K.-h. Lam, B. Huang, Q. Wang and Y. Zhao, Defect-engineered reduced graphene oxide sheets with high electric conductivity and controlled thermal conductivity for soft and flexible wearable thermoelectric generators, *Nano Energy*, 2018, **54**, 163–174.
- 95 S. L. Kim, J.-H. Hsu and C. Yu, Intercalated graphene oxide for flexible and practically large thermoelectric voltage generation and simultaneous energy storage, *Nano Energy*, 2018, **48**, 582–589.
- 96 Z. Yang, F. Dang, C. Zhang, S. Sun, W. Zhao, X. Li, Y. Liu and X. Chen, Harvesting Low-Grade Heat via Thermal-Induced Electric Double Layer Redistribution of Nanoporous Graphene Films, *Langmuir*, 2019, **35**(24), 7713–7719.
- 97 C. Hou, H. Wang, Q. Zhang, Y. Li and M. Zhu, Highly Conductive, Flexible, and Compressible All-Graphene Passive Electronic Skin for Sensing Human Touch, *Adv. Mater.*, 2014, **26**(29), 5018–5024.
- 98 D. Zhang, K. Zhang, Y. Wang, Y. Wang and Y. Yang, Thermoelectric effect induced electricity in stretchable graphene-polymer nanocomposites for ultrasensitive self-powered strain sensor system, *Nano Energy*, 2019, **56**, 25–32.
- 99 M. A. Al Faruque, M. Syduzzaman, J. Sarkar, K. Bilisik and M. Naebe, A Review on the Production Methods and Applications of Graphene-Based Materials, *Nanomaterials*, 2021, **11**(9), 2414.
- 100 J. Wang, X. Mu and M. Sun, The Thermal, Electrical and Thermoelectric Properties of Graphene Nanomaterials, *Nanomaterials*, 2019, **9**(2), 218.
- 101 T. A. Amollo, G. T. Mola, M. S. K. Kirui and V. O. Nyamori, Graphene for Thermoelectric Applications: Prospects and





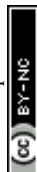
- Challenges, *Crit. Rev. Solid State Mater. Sci.*, 2018, **43**(2), 133–157.
- 102 K. S. Novoselov, A. K. Geim, S. V. Morozov, D. Jiang, M. I. Katsnelson, I. V. Grigorieva, S. V. Dubonos and A. A. Firsov, Two-dimensional gas of massless Dirac fermions in graphene, *Nature*, 2005, **438**(7065), 197–200.
  - 103 A. K. Geim and K. S. Novoselov, The rise of graphene, *Nat. Mater.*, 2007, **6**(3), 183–191.
  - 104 J. G. Checkelsky and N. P. Ong, Thermopower and Nernst effect in graphene in a magnetic field, *Phys. Rev. B: Condens. Matter Mater. Phys.*, 2009, **80**(8), 081413.
  - 105 D. Wang and J. Shi, Effect of charged impurities on the thermoelectric power of graphene near the Dirac point, *Phys. Rev. B: Condens. Matter Mater. Phys.*, 2011, **83**(11), 113403.
  - 106 Y. Anno, Y. Imakita, K. Takei, S. Akita and T. Arie, Enhancement of graphene thermoelectric performance through defect engineering, *2D Mater.*, 2017, **4**(2), 025019.
  - 107 G. Lim, K. D. Kihm, H. G. Kim, W. Lee, W. Lee, K. R. Pyun, S. Cheon, P. Lee, J. Y. Min and S. H. Ko, Enhanced Thermoelectric Conversion Efficiency of CVD Graphene with Reduced Grain Sizes, *Nanomaterials*, 2018, **8**(7), 557.
  - 108 W. Lee, K. D. Kihm, H. G. Kim, S. Shin, C. Lee, J. S. Park, S. Cheon, O. M. Kwon, G. Lim and W. Lee, In-Plane Thermal Conductivity of Polycrystalline Chemical Vapor Deposition Graphene with Controlled Grain Sizes, *Nano Lett.*, 2017, **17**(4), 2361–2366.
  - 109 H. Sevinçli and G. Cuniberti, Enhanced thermoelectric figure of merit in edge-disordered zigzag graphene nanoribbons, *Phys. Rev. B: Condens. Matter Mater. Phys.*, 2010, **81**(11), 113401.
  - 110 P. Dollfus, V. Hung Nguyen and J. Saint-Martin, Thermoelectric effects in graphene nanostructures, *J. Phys.: Condens. Matter*, 2015, **27**(13), 133204.
  - 111 M. Yamawaki, M. Ohnishi, S. Ju and J. Shiomi, Multi-functional structural design of graphene thermoelectrics by Bayesian optimization, *Science*, 2018, **4**(6), eaar4192.
  - 112 J. Palacios, J. Fernández-Rossier, L. Brey and H. A. Fertig, Electronic and magnetic structure of graphene nanoribbons, *Semicond. Sci. Technol.*, 2010, **25**(3), 033003.
  - 113 W. Choi, I. Lahiri, R. Seelaboyina and Y. S. Kang, Synthesis of graphene and its applications: a review, *Crit. Rev. Solid State Mater. Sci.*, 2010, **35**(1), 52–71.
  - 114 Y. Anno, K. Takei, S. Akita and T. Arie, Enhancing the Thermoelectric Device Performance of Graphene Using Isotopes and Isotopic Heterojunctions, *Adv. Electron. Mater.*, 2015, **1**(9), 1500175.
  - 115 Y. Xu, Z. Li and W. Duan, Thermal and Thermoelectric Properties of Graphene, *Small*, 2014, **10**(11), 2182–2199.
  - 116 H. Zhang, G. Lee, A. F. Fonseca, T. L. Borders and K. Cho, Isotope Effect on the Thermal Conductivity of Graphene, *J. Nanomater.*, 2010, **2010**, 537657.
  - 117 E. Pop, V. Varshney and A. K. Roy, Thermal properties of graphene: Fundamentals and applications, *MRS Bull.*, 2012, **37**(12), 1273–1281.
  - 118 R. Gopal, P. Narayanan and A. Parashar, Effect of Point and Line Defects on Mechanical and Thermal Properties of Graphene: A Review, *Crit. Rev. Solid State Mater. Sci.*, 2015, **41**, 47–71.
  - 119 D. Huang, H. Yao, Y. Cui, Y. Zou, F. Zhang, C. Wang, H. Shen, W. Jin, J. Zhu, Y. Diao, W. Xu, C.-a. Di and D. Zhu, Conjugated-Backbone Effect of Organic Small Molecules for n-Type Thermoelectric Materials with ZT over 0.2, *J. Am. Chem. Soc.*, 2017, **139**(37), 13013–13023.
  - 120 G. Wu, C. Gao, G. Chen, X. Wang and H. Wang, High-performance organic thermoelectric modules based on flexible films of a novel n-type single-walled carbon nanotube, *J. Mater. Chem. A*, 2016, **4**(37), 14187–14193.
  - 121 D. S. Montgomery, C. A. Hewitt, R. Barbalace, T. Jones and D. L. Carroll, Spray doping method to create a low-profile high-density carbon nanotube thermoelectric generator, *Carbon*, 2016, **96**, 778–781.
  - 122 M. Bharti, A. Singh, A. Debnath, A. Chauhan, K. Muthe, S. Gupta, K. Marumoto, T. Mori and D. J. Aswal, Anionic conduction mediated giant n-type Seebeck coefficient in doped Poly(3-hexylthiophene) free-standing films, *Mater. Today Phys.*, 2021, **16**, 100307.
  - 123 L. Wang, Q. Yao, H. Bi, F. Huang, Q. Wang and L. Chen, Large thermoelectric power factor in polyaniline/graphene nanocomposite films prepared by solution-assistant dispersing method, *J. Mater. Chem. A*, 2014, **2**(29), 11107–11113.
  - 124 T. Ube, J. Koyanagi, T. Kosaki, K. Fujimoto, T. Yokozeki, T. Ishiguro and K. Nishio, Fabrication of well-isolated graphene and evaluation of thermoelectric performance of polyaniline-graphene composite film, *J. Mater. Sci.*, 2019, **54**(5), 3904–3913.
  - 125 C. Yu, Y. S. Kim, D. Kim and J. C. Grunlan, Thermoelectric behavior of segregated-network polymer nanocomposites, *Nano Lett.*, 2008, **8**(12), 4428–4432.
  - 126 B. Abad, I. Alda, P. Díaz-Chao, H. Kawakami, A. Almarza, D. Amantia, D. Gutierrez, L. Aubouy and M. Martín-González, Improved power factor of polyaniline nanocomposites with exfoliated graphene nanoplatelets (GNPs), *J. Mater. Chem. A*, 2013, **1**(35), 10450–10457.
  - 127 K. Zhang, Y. Zhang and S. Wang, Enhancing thermoelectric properties of organic composites through hierarchical nanostructures, *Sci. Rep.*, 2013, **3**(1), 3448.
  - 128 Y. Lu, Y. Song and F. Wang, Thermoelectric properties of graphene nanosheets-modified polyaniline hybrid nanocomposites by an *in situ* chemical polymerization, *Mater. Chem. Phys.*, 2013, **138**(1), 238–244.
  - 129 K. Zhang, Y. Zhang and S. Wang, Enhancing thermoelectric properties of organic composites through hierarchical nanostructures, *Sci. Rep.*, 2013, **3**(1), 3448.
  - 130 G. H. Kim, D. H. Hwang and S. I. Woo, Thermoelectric properties of nanocomposite thin films prepared with poly(3, 4-ethylenedioxythiophene) poly(styrenesulfonate) and graphene, *Phys. Chem. Chem. Phys.*, 2012, **14**(10), 3530–3536.
  - 131 D. Yoo, J. Kim and J. H. Kim, Direct synthesis of highly conductive poly(3, 4-ethylenedioxythiophene): poly(4-styrenesulfonate)(PEDOT: PSS)/graphene composites and



- their applications in energy harvesting systems, *Nano Res.*, 2014, 7, 717–730.
- 132 J. Xiang and L. T. Drzal, Templated growth of polyaniline on exfoliated graphene nanoplatelets (GNP) and its thermoelectric properties, *Polymer*, 2012, 53(19), 4202–4210.
  - 133 Y. Du, S. Z. Shen, W. Yang, R. Donelson, K. Cai and P. S. Casey, Simultaneous increase in conductivity and Seebeck coefficient in a polyaniline/graphene nanosheets thermoelectric nanocomposite, *Synth. Met.*, 2012, 161(23–24), 2688–2692.
  - 134 G. Decher, *Multilayer Thin Films: Sequential Assembly of Nanocomposite Materials*, 2003, pp. 1–46.
  - 135 D. Zhang, Y. Mao, P. Bai, Q. Li, W. He, H. Cui, F. Ye, C. Li, R. Ma and Y. Chen, Multifunctional Superelastic Graphene-Based Thermoelectric Sponges for Wearable and Thermal Management Devices, *Nano Lett.*, 2022, 22(8), 3417–3424.
  - 136 K. Zhang, Y. Zhang and S. Wang, Enhancing thermoelectric properties of organic composites through hierarchical nanostructures, *Sci. Rep.*, 2013, 3, 3448.
  - 137 C. Cho, B. Stevens, J.-H. Hsu, R. Bureau, D. A. Hagen, O. Regev, C. Yu and J. C. Grunlan, Completely Organic Multilayer Thin Film with Thermoelectric Power Factor Rivaling Inorganic Tellurides, *Adv. Mater.*, 2015, 27(19), 2996–3001.
  - 138 G. H. Kim, D. H. Hwang and S. I. Woo, Thermoelectric properties of nanocomposite thin films prepared with poly(3,4-ethylenedioxythiophene) poly(styrenesulfonate) and graphene, *Phys. Chem. Chem. Phys.*, 2012, 14(10), 3530–3536.
  - 139 J. Xiang and L. T. Drzal, Templated growth of polyaniline on exfoliated graphene nanoplatelets (GNP) and its thermoelectric properties, *Polymer*, 2012, 53(19), 4202–4210.
  - 140 S.-H. Hwang, H. W. Park and Y.-B. Park, Piezoresistive behavior and multi-directional strain sensing ability of carbon nanotube–graphene nanoplatelet hybrid sheets, *Smart Mater. Struct.*, 2012, 22(1), 015013.
  - 141 H. X. Kong, Hybrids of carbon nanotubes and graphene/graphene oxide, *Curr. Opin. Solid State Mater. Sci.*, 2013, 17(1), 31–37.
  - 142 W. Li, D. He and J. Bai, The influence of nano/micro hybrid structure on the mechanical and self-sensing properties of the carbon nanotube-microparticle reinforced epoxy composites, *Composites, Part A*, 2013, 54, 28–36.
  - 143 Q. Wang, Q. Yao, J. Chang and L. Chen, Enhanced thermoelectric properties of CNT/PANI composite nanofibers by highly orienting the arrangement of polymer chains, *J. Mater. Chem.*, 2012, 22(34), 17612–17618.
  - 144 D. Yoo, J. Kim and J. H. Kim, Direct synthesis of highly conductive poly(3,4-ethylenedioxythiophene):poly(4-styrenesulfonate) (PEDOT:PSS)/graphene composites and their applications in energy harvesting systems, *Nano Res.*, 2014, 7(5), 717–730.
  - 145 Y. Du, S. Z. Shen, W. D. Yang, K. F. Cai and P. S. Casey, Preparation and characterization of multiwalled carbon nanotube/poly(3-hexylthiophene) thermoelectric composite materials, *Synth. Met.*, 2012, 162(3), 375–380.
  - 146 Y. Du, J. Li, J. Xu and P. Eklund, Thermoelectric Properties of Reduced Graphene Oxide/Bi<sub>2</sub>Te<sub>3</sub> Nanocomposites, *Energies*, 2019, 12(12), 2430.
  - 147 J. Dong, W. Liu, H. Li, X. Su, X. Tang and C. Uher, *In situ* synthesis and thermoelectric properties of PbTe–graphene nanocomposites by utilizing a facile and novel wet chemical method, *J. Mater. Chem. A*, 2013, 1(40), 12503–12511.
  - 148 H. Ju, M. Kim and J. Kim, A facile fabrication of n-type Bi<sub>2</sub>Te<sub>3</sub> nanowire/graphene layer-by-layer hybrid structures and their improved thermoelectric performance, *Chem. Eng. J.*, 2015, 275, 102–112.
  - 149 K. Agarwal, V. Kaushik, D. Varandani, A. Dhar and B. R. Mehta, Nanoscale thermoelectric properties of Bi<sub>2</sub>Te<sub>3</sub> – Graphene nanocomposites: Conducting atomic force, scanning thermal and kelvin probe microscopy studies, *J. Alloys Compd.*, 2016, 681, 394–401.
  - 150 S. Kumar, S. Singh, P. K. Dhawan, R. R. Yadav and N. Khare, Effect of graphene nanofillers on the enhanced thermoelectric properties of Bi<sub>2</sub>Te<sub>3</sub> nanosheets: elucidating the role of interface in de-coupling the electrical and thermal characteristics, *Nanotechnology*, 2018, 29(13), 135703.
  - 151 Y. Zhang, H. Ma, B. Sun, B. Liu, H. Liu, L. Kong, B. Liu, X. Jia and X. Chen, Thermoelectric performance of graphene composited BiSbTe bulks by high pressure synthesis, *J. Alloys Compd.*, 2017, 715, 344–348.
  - 152 H. Ju and J. Kim, Preparation and structure dependent thermoelectric properties of nanostructured bulk bismuth telluride with graphene, *J. Alloys Compd.*, 2016, 664, 639–647.
  - 153 W. H. Shin, K. Ahn, M. Jeong, J. S. Yoon, J. M. Song, S. Lee, W. S. Seo and Y. S. Lim, Enhanced thermoelectric performance of reduced graphene oxide incorporated bismuth-antimony-telluride by lattice thermal conductivity reduction, *J. Alloys Compd.*, 2017, 718, 342–348.
  - 154 B. Liang, Z. Song, M. Wang, L. Wang and W. Jiang, Fabrication and Thermoelectric Properties of Graphene Composite Materials, *J. Nanomater.*, 2013, 2013, 210767.
  - 155 Y. Wang, H. Pang, Q. Guo, N. Tsujii, T. Baba, T. Baba and T. Mori, Flexible n-Type Abundant Chalcopyrite/PEDOT:PSS/Graphene Hybrid Film for Thermoelectric Device Utilizing Low-Grade Heat, *ACS Appl. Mater. Interfaces*, 2021, 13(43), 51245–51254.
  - 156 K. R. Nandanapalli, D. Mudusu, J. Bae, W. Jeong, G. D. Moon and S. Lee, Larger, flexible, and skin-mountable energy devices with graphene single layers for integratable, wearable, and health monitoring systems, *Materials Today, Chemistry*, 2022, 23, 100764.
  - 157 J. Gobpant, N. Somdock, P. Limsuwan, A. Sakulkalavek and R. Sakdanuphab, Graphene addition improved figure of merit in SnTe prepared by the rapid hybrid microwave solid-state method, *J. Phys. Chem. Solids*, 2022, 161, 110490.
  - 158 W. Wang, Q. Zhang, J. Li, X. Liu, L. Wang, J. Zhu, W. Luo and W. Jiang, An efficient thermoelectric material: preparation of reduced graphene oxide/polyaniline hybrid



- composites by cryogenic grinding, *RSC Adv.*, 2015, 5(12), 8988–8995.
- 159 S. Xin, N. Yang, F. Gao, J. Zhao, L. Li and C. Teng, Free-standing and flexible polypyrrole nanotube/reduced graphene oxide hybrid film with promising thermoelectric performance, *Mater. Chem. Phys.*, 2018, **212**, 440–445.
  - 160 M. K. Ali, A. Hessein, M. A. Hassan, M. Ghali, N. M. Shaalan, K. Nakamura and A. A. El-Moneim, Heteroatom-doped reduced graphene oxide/polyaniline nanocomposites with improved n-type thermoelectric performance, *J. Appl. Polym. Sci.*, 2021, **138**(34), 50852.
  - 161 H. Song, C. Liu, H. Zhu, F. Kong, B. Lu, J. Xu, J. Wang and F. Zhao, Improved Thermoelectric Performance of Free-Standing PEDOT:PSS/Bi<sub>2</sub>Te<sub>3</sub> Films with Low Thermal Conductivity, *J. Electron. Mater.*, 2013, **42**(6), 1268–1274.
  - 162 G. S. Hegde, V. Parol, A. Rao, A. N. Prabhu, J. J. B. Levinsky and G. R. Blake, Thermoelectric properties of co-doped (Bi<sub>0.98</sub>In<sub>0.02</sub>)<sub>2</sub>Te<sub>2.7</sub>Se<sub>0.3</sub>/reduced graphene oxide composites prepared by solid-state reaction, *Mater. Res. Bull.*, 2022, **145**, 111517.
  - 163 G. Kim, S. W. Kim, H. J. Rim, H. Lee, J. Kim, J. W. Roh, B.-W. Kim, K. H. Lee and W. Lee, Improved trade-off between thermoelectric performance and mechanical reliability of Mg<sub>2</sub>Si by hybridization of few-layered reduced graphene oxides, *Scr. Mater.*, 2019, **162**, 402–407.
  - 164 K. Ahmad and C. Wan, Enhanced thermoelectric performance of Bi<sub>2</sub>Te<sub>3</sub> through uniform dispersion of single wall carbon nanotubes, *Nanotechnology*, 2017, **28**(41), 415402.
  - 165 B. Zhang, J. Sun, H. E. Katz, F. Fang and R. L. Opila, Promising thermoelectric properties of commercial PEDOT:PSS materials and their bi<sub>2</sub>Te<sub>3</sub> powder composites, *ACS Appl. Mater. Interfaces*, 2010, **2**(11), 3170–3178.
  - 166 A. Dey, O. P. Bajpai, A. K. Sikder, S. Chattopadhyay and M. A. S. Khan, Recent advances in CNT/graphene based thermoelectric polymer nanocomposite: A proficient move towards waste energy harvesting, *Renewable Sustainable Energy Rev.*, 2016, **53**, 653–671.
  - 167 S. L. Kim, K. Choi, A. Tazebay and C. Yu, Flexible Power Fabrics Made of Carbon Nanotubes for Harvesting Thermoelectricity, *ACS Nano*, 2014, **8**(3), 2377–2386.
  - 168 C. A. Hewitt, A. B. Kaiser, S. Roth, M. Craps, R. Czerw and D. L. Carroll, Multilayered Carbon Nanotube/Polymer Composite Based Thermoelectric Fabrics, *Nano Lett.*, 2012, **12**(3), 1307–1310.
  - 169 Y. Du, K. F. Cai, S. Z. Shen, R. Donelson and J. Y. Xu, H. X. Wang and T. Lin, Multifold enhancement of the output power of flexible thermoelectric generators made from cotton fabrics coated with conducting polymer, *RSC Adv.*, 2017, **7**(69), 43737–43742.
  - 170 W. Zhou, Q. Fan, Q. Zhang, L. Cai, K. Li, X. Gu, F. Yang, N. Zhang, Y. Wang, H. Liu, W. Zhou and S. Xie, High-performance and compact-designed flexible thermoelectric modules enabled by a reticulate carbon nanotube architecture, *Nat. Commun.*, 2017, **8**, 14886.
  - 171 B. Dörfling, J. D. Ryan, J. D. Craddock, A. Sorrentino, A. E. Basaty, A. Gomez, M. Garriga, E. Pereiro, J. E. Anthony, M. C. Weisenberger, A. R. Goñi, C. Müller and M. Campoy-Quiles, Photoinduced p- to n-type Switching in Thermoelectric Polymer-Carbon Nanotube Composites, *Adv. Mater.*, 2016, **28**(14), 2782–2789.
  - 172 Q. Yao, L. Chen, W. Zhang, S. Liufu and X. Chen, Enhanced thermoelectric performance of single-walled carbon nanotubes/polyaniline hybrid nanocomposites, *ACS Nano*, 2010, **4**(4), 2445–2451.
  - 173 L. Wang, D. Wang, G. Zhu, J. Li and F. Pan, Thermoelectric properties of conducting polyaniline/graphite composites, *Mater. Lett.*, 2011, **65**, 1086–1088.
  - 174 S. Kirkpatrick, Percolation and Conduction, *Rev. Mod. Phys.*, 1973, **45**(4), 574–588.
  - 175 C. Meng, C. Liu and S. Fan, A Promising Approach to Enhanced Thermoelectric Properties Using Carbon Nanotube Networks, *Adv. Mater.*, 2010, **22**(4), 535–539.
  - 176 R. C. Y. King, F. Roussel, J.-F. Brun and C. Gors, Carbon nanotube-polyaniline nanohybrids: influence of the carbon nanotube characteristics on the morphological, spectroscopic, electrical and thermoelectric properties, *Synth. Met.*, 2012, **162**(15–16), 1348–1356.
  - 177 M. S. Islam, H. Ohmagari, M. A. Rahman, Y. Shudo, M. Fukuda, J. Yagyu, Y. Sekine, L. F. Lindoy and S. Hayami, Enhanced thermoelectric properties exhibited by unreduced freestanding graphene oxide/carbon nanotube membranes, *Mater. Adv.*, 2021, **2**(17), 5645–5649.
  - 178 L. Wang, Z. Zhang, L. Geng, T. Yuan, Y. Liu, J. Guo, L. Fang, J. Qiu and S. Wang, Solution-printable fullerene/TiS<sub>2</sub> organic/inorganic hybrids for high-performance flexible n-type thermoelectrics, *Energy Environ. Sci.*, 2018, **11**(5), 1307–1317.
  - 179 H. Fang, B. C. Popere, E. M. Thomas, C. K. Mai, W. B. Chang, G. C. Bazan, M. L. Chabinyc and R. A. Segalman, Large-scale integration of flexible materials into rolled and corrugated thermoelectric modules, *J. Appl. Polym. Sci.*, 2017, **134**(3), 44208.
  - 180 F. Soltani-kordshuli, F. Zabihi and M. Eslamian, Graphene-doped PEDOT: PSS nanocomposite thin films fabricated by conventional and substrate vibration-assisted spray coating (SVASC), *Eng., Sci. Technol. Int. J.*, 2016, **19**(3), 1216–1223.
  - 181 M. Acik, G. Lee, C. Mattevi, A. Pirkle, R. M. Wallace, M. Chhowalla, K. Cho and Y. Chabal, The Role of Oxygen during Thermal Reduction of Graphene Oxide Studied by Infrared Absorption Spectroscopy, *J. Phys. Chem. C*, 2011, **115**(40), 19761–19781.
  - 182 J.-S. Yeo, J.-M. Yun, D.-Y. Kim, S. Park, S.-S. Kim, M.-H. Yoon, T.-W. Kim and S.-I. Na, Significant Vertical Phase Separation in Solvent-Vapor-Annealed Poly(3,4-ethylenedioxythiophene):Poly(styrene sulfonate) Composite Films Leading to Better Conductivity and Work Function for High-Performance Indium Tin Oxide-Free Optoelectronics, *ACS Appl. Mater. Interfaces*, 2012, **4**(5), 2551–2560.
  - 183 W. Hong, Y. Xu, G. Lu, C. Li and G. Shi, Transparent graphene/PEDOT-PSS composite films as counter



- electrodes of dye-sensitized solar cells, *Electrochem. Commun.*, 2008, **10**(10), 1555–1558.
- 184 F.-P. Du, N.-N. Cao, Y.-F. Zhang, P. Fu, Y.-G. Wu, Z.-D. Lin, R. Shi, A. Amini and C. Cheng, PEDOT: PSS/graphene quantum dots films with enhanced thermoelectric properties *via* strong interfacial interaction and phase separation, *Sci. Rep.*, 2018, **8**(1), 6441.
  - 185 T. Juntunen, H. Jussila, M. Ruoho, S. Liu, G. Hu, T. Albrow-Owen, L. W. T. Ng, R. C. T. Howe, T. Hasan, Z. Sun and I. Tittonen, Inkjet Printed Large-Area Flexible Few-Layer Graphene Thermoelectrics, *Adv. Funct. Mater.*, 2018, **28**(22), 1800480.
  - 186 H. Alam and S. J. N. E. Ramakrishna, A review on the enhancement of figure of merit from bulk to nano-thermoelectric materials, *Nano Energy*, 2013, **2**(2), 190–212.
  - 187 C. Walse, B. Berg and H. Sverdrup, Review and synthesis of experimental data on organic matter decomposition with respect to the effect of temperature, moisture, and acidity, *Environ. Rev.*, 1998, **6**(1), 25–40.
  - 188 S. J. Zinkle and G. Was, Materials challenges in nuclear energy, *Acta Biomater.*, 2013, **61**(3), 735–758.
  - 189 J. Porter, A. Laveron-Simavilla, M. Bou-Ali, X. Ruiz, F. Gavalda, J. Ezquerro, P. S. Sánchez, U. Martínez, D. Gligor and I. Tinao, The “Effect of Marangoni Convection on Heat Transfer in Phase Change Materials” experiment, *Acta Astronaut.*, 2023, **210**, 212–223.
  - 190 G. Lanzavecchia, J. Kuttruff, A. Doricchi, A. Douaki, K. Kumaranchira Ramankutty, I. García, L. Lin, A. Viejo Rodríguez, T. Wågberg and R. Krahne, Plasmonic Photochemistry as a Tool to Prepare Metallic Nanopores with Controlled Diameter for Optimized detection of single entities, *Adv. Opt. Mater.*, 2023, 2300786.
  - 191 H. Li, C. Zhang, P. Li, S. Liu, H. Zhang and C. He, Recent development in flexible organic thermoelectric fibers for wearable devices, *Mater. Today Chem.*, 2023, **34**, 101774.
  - 192 A. G. Adeniyi, K. O. Iwuzor, E. C. Emenike, P. A. Sagboye, K. T. Micheal, T. T. Micheal, O. D. Saliu and R. James, Biomass-derived activated carbon monoliths: A review of production routes, performance, and commercialization potential, *J. Cleaner Prod.*, 2023, 138711.
  - 193 J. He, K. Li, L. Jia, Y. Zhu, H. Zhang and J. Linghu, Advances in the Applications of Thermoelectric Generators, *Appl. Therm. Eng.*, 2023, 121813.
  - 194 A. Patel, Optimizing the Efficiency of Solar Heater and Heat Exchanger Integration in Hybrid System, *TJER Int. Res. J.*, 2023, 2349–9249.
  - 195 L. Novoveská, S. L. Nielsen, O. T. Eroldoğan, B. Z. Haznedaroglu, B. Rinkevich, S. Fazi, J. Robbens, M. Vasquez and H. Einarsson, Overview and challenges of large-scale cultivation of photosynthetic microalgae and cyanobacteria, *Mar. Drugs*, 2023, **21**(8), 445.
  - 196 H. H. Shi, Y. Pan, L. Xu, X. Feng, W. Wang, P. Potluri, L. Hu, T. Hasan and Y. Y. S. Huang, Sustainable electronic textiles towards scalable commercialization, *Nat. Mater.*, 2023, 1–10.
  - 197 M. Abolhasani and E. Kumacheva, The rise of self-driving labs in chemical and materials sciences, *Nat. Synth.*, 2023, 1–10.
  - 198 A. Mohammad and F. Mahjabeen, From Silicon to Sunlight: Exploring the Evolution of Solar Cell Materials, *JURIHUM: Jurnal Inovasi dan Humaniora*, 2023, **1**(2), 316–330.
  - 199 H. Alghamdi, C. Maduabuchi, K. Okoli, A. Albaker, I. Alatawi, A. S. Alsafran, M. Alkhedher and W.-H. Chen, Smart optimization of semiconductors in photovoltaic-thermoelectric systems using recurrent neural networks, *Int. J. Energy Res.*, 2023, **2023**, DOI: [10.1155/2023/6927245](https://doi.org/10.1155/2023/6927245).
  - 200 T. Kucova, M. Prauzek, J. Konecny, D. Andriukaitis, M. Zilys and R. Martinek, Thermoelectric energy harvesting for internet of things devices using machine learning: A review, *CAAI Trans. Intell. Technol.*, 2023, **8**(3), 680–700.

